



## Development of nano-silver doped zeolite A synthesized from Nigerian Ahoko kaolin for treatment of wastewater of a typical textile company

S. Alaya-Ibrahim, A. S. Kovo, A. S. Abdulkareem, O. D. Adeniyi & M. D. Yahya

To cite this article: S. Alaya-Ibrahim, A. S. Kovo, A. S. Abdulkareem, O. D. Adeniyi & M. D. Yahya (2019): Development of nano-silver doped zeolite A synthesized from Nigerian Ahoko kaolin for treatment of wastewater of a typical textile company, Chemical Engineering Communications, DOI: [10.1080/00986445.2019.1641490](https://doi.org/10.1080/00986445.2019.1641490)

To link to this article: <https://doi.org/10.1080/00986445.2019.1641490>



Published online: 23 Jul 2019.



Submit your article to this journal [↗](#)



View Crossmark data [↗](#)



## Development of nano-silver doped zeolite A synthesized from Nigerian Ahoko kaolin for treatment of wastewater of a typical textile company

S. Alaya-Ibrahim<sup>a,b</sup>, A. S. Kovo<sup>a,b,c</sup>, A. S. Abdulkareem<sup>a,b</sup>, O. D. Adeniyi<sup>b</sup>, and M. D. Yahya<sup>b</sup>

<sup>a</sup>Nanotechnology Group, Centre for Biotechnology and Genetic Engineering, Federal University of Technology, Niger State, Nigeria;

<sup>b</sup>Chemical Engineering Department, Federal University of Technology, Minna, Niger State, Nigeria; <sup>c</sup>Department of Chemistry, University of Bath, Bath, United Kingdom

### ABSTRACT

In this work, nano-silver synthesized with mango leaf extract as a reducing agent was doped onto synthesized zeolite A (SZA), produced from Nigerian kaolin via green synthesis route. The produced adsorbents were characterized using X-ray fluorescence (XRF), X-ray powder diffraction (XRD), high-resolution transmission electron microscopy (HRTEM), Fourier-transform infrared spectroscopy (FTIR) and Brunauer–Emmett–Teller (BET) surface analysis, in addition, it is to be used for the treatment of local textile effluent. The physicochemical parameters of the effluent were analyzed using standard methods. The HRTEM micrographs revealed well dispersed AgNPs on SZA and the BET surface area revealed high surface areas of 119.98 m<sup>2</sup>/g and 436.44 m<sup>2</sup>/g for SZA and silver-doped zeolite A (SDZA), respectively. The array of removal of the pollutants was BOD > COD > CN<sup>-</sup> > Cl<sup>-</sup> > NO<sub>2</sub><sup>-</sup> > TOC for SZA and CN<sup>-</sup> > BOD > COD > NO<sub>2</sub><sup>-</sup> > Cl<sup>-</sup> > TOC for SDZA, with the doped adsorbent removing the higher pollutants in all cases. Isothermal models indicated that Jovanovic model ( $R^2 > 0.999$ ) was most suitable for describing the adsorption process, which conformed to pseudo-second order kinetics with intraparticle diffusion of micropore type. The thermodynamic studies showed spontaneous and endothermic reactions.

### KEYWORDS



Ahoko; characterization; chemical parameters; kaolin; nano-silver doped zeolite A; textile wastewater

### Introduction

The adverse effect of untreated effluents on the environment has necessitated the governments of most countries to impose stringent legislations for treatment of industrial effluents before disposal (Dey and Islam, 2015). This is because globalization, urbanization, and industrialization have led to an increase in environmental pollution, which is currently one of the most important issues facing humanity (Dey and Islam, 2015). The most common and dangerous pollutants which are discharged in large quantities from dye manufacturing, textile, pulp and paper industries are dyes, pigments, and heavy metals. Textiles industries have been known to be major contributor to environmental pollution with more than 200 types of chemicals and over 7000 types of dyes being used by them (Al-Asheh et al., 2003). In addition, textile industries involve

various wet processes such as desizing, scouring, bleaching, mercerizing, dyeing and finishing, resulting in large amounts of wastewater being generated which is not treated prior to its discharge into the surface water (Tafesse et al., 2015). Unfortunately, this contaminated surface water serves as a source of farm irrigation in developing countries like Nigeria.

Although, the key physicochemical constraints of textile effluent have been recognized as dyes (color), odor, pH, total dissolved solids (TDS), dissolved oxygen (DO), chemical oxygen demand (COD), biochemical oxygen demand (BOD), and electrical conductivity (Tafesse et al., 2015). However, the detrimental effect of other pollutants such as suspended solids, heavy metals, and other supporting chemicals in the like of chloride, nitrites, nitrates, cyanide, phosphate, and fluoride cannot be ignored. They are known to

**CONTACT** A. S. Kovo  kvo@futminna.edu.ng  Nanotechnology Group, Centre for Biotechnology and Genetic Engineering, Federal University of Technology, PMB 65, Minna, Niger State, Nigeria.

Color versions of one or more of the figures in the article can be found online at [www.tandfonline.com/gcec](http://www.tandfonline.com/gcec).

© 2019 Taylor & Francis Group, LLC

be toxic and potentially carcinogenic (Kant, 2011; Bertolini et al., 2013). For instance, high chloride water can destroy microorganisms required to maintain food chains in aquatic life (Elango et al., 2017), high BOD, COD, and TOC lead to inadequate oxygen for living organisms in the water, which also poses threat to human life and the environment (Patel et al., 2015). Thus, there is a need to search for low-cost adsorbents and effective technologies for the treatment of textile industries wastewater.

Of the technologies used in treatment of wastewater, adsorption techniques have proven to be the most effective and efficient (Piccin et al., 2011; Dada et al., 2012; Yusuf-Alaya, 2014; Bankole et al., 2017). One such adsorbent which has received much interest in this application is zeolite A, due to its low-cost and versatile range of properties (Zavareh et al., 2018). Furthermore, this zeolite A is capable of undergoing functionalization/doping in order to enhance its surface properties for enhanced adsorption efficiency (Mabape, 2017). Doping is required because of many non-biodegradable pollutants present in the textile effluent which cannot be removed at the same rate (Mabape, 2017). However, while many researchers have worked on the removal of pollutants from textile effluents, the doping techniques used have made use of chemical surfactants which are actually more hazardous to the environment, due to the by-products generated from the process (Chouhan et al., 2013; Juliano and Magrini, 2017). Thus, doping the adsorbent using a green synthesis route is a necessity.

Recently, metallic nanoparticles are gaining attention due to their application in various fields especially in water treatment. The most important fields of research in nanotechnology are the synthesis of different nanoparticles such as gold, silver, iron, among others (Mittal et al., 2013; Muthoosany et al., 2015; Allafchian et al., 2016). Silver nanoparticles have spherical or flake morphology with high surface area, typically of 1–40 nm with an average particle size of 2–10-microns. They usually have much larger surface areas than bulk particles which make them applicable in water remediation and treatment. However, among the techniques used in synthesizing nanoparticles, biosynthesis using plant

extract is receiving considerable attention due to numerous advantages such as low cost, environmental friendliness, readiness for scalability and availability (Allafchian et al., 2016).

This study focuses on using a biosynthesis route in doping silver nanoparticles on the surface of zeolite A developed from Ahoko kaolin for treatment of textile wastewater (TWW).

## Materials and methods

### Materials

The kaolin used in this work was collected from Ahoko, Kogi state, Nigeria;  $\text{AgNO}_3$  salt is of analytical grade, manufactured by Sigma-Aldrich, St. Louis, MO, USA. Deionized and distilled water were used throughout the study and the mango leaves were collected from Tunga area of Minna, Niger state, Nigeria.

### Refining of the raw kaolin

The refining process started by crushing 500 g of the raw Ahoko (AH) kaolin using a porcelain mortar and pestle. It was then soaked in 5 L of distilled water for 24 h. After which, the dissolved kaolin was properly stirred for another 1 h to obtain a homogeneous mixture. The slurry was transferred into an aspirator bottle which serves as the settling tank. Stokes settling time equation was used to calculate the settling time as shown in Equation (1).

$$t = \frac{18\eta H}{D^2 g(\rho_p - \rho_w)} \quad (1)$$

where,  $D$  is the particles diameter,  $G$  is gravitational constant,  $\rho_p$  is the particle density,  $\rho_w$  is water density,  $\eta$  is viscosity of water,  $t$  is settling time and  $H$  is the distance traveled.

The settling time of the heavier component was calculated to be 17 h 15 min using a settling height of 25 cm. At the end of the settling time, the heavier component (quartz) with size  $> 2 \mu\text{m}$  naturally settled and the lighter fraction with size  $< 2 \mu\text{m}$  remained as supernatant. The supernatant (kaolin fraction) was collected and allowed to settle for 1 week. The settled clay sample was collected and dried in an oven at a temperature of  $80^\circ\text{C}$  for 12 h. The refined kaolin was

characterized using X-ray powder diffraction (XRD), scanning electron microscope (SEM), and X-ray fluorescence (XRF).

### **Metakaolinization process**

The metakaolinization process was carried out by crushing the refined kaolin mildly with a porcelain mortar and pestle, after which it was screened using 75  $\mu\text{m}$  meshes. 50 g of the sieved sample was weighed and kept in crucibles while the muffle furnace was heated to a temperature of 600 °C at the rate of 10 °C/min as soon as it reached the 600 °C, the crucibles containing the weighed sample were loaded into the furnace for 1 h. After which the samples were removed and allowed to cool in air. XRD, SEM, and XRF were used for its characterization.

### **Synthesis of zeolites a from metakaolin**

The synthesis of Zeolite A was based on our previous work (Yusuf-Alaya, 2014) with little modifications. The synthesis gel was formed by dissolving 6.6 g of NaOH in 60 mL of distilled water and 5.7 g of metakaolin was added to it. The resulting gel was aged at room temperature for 6 h on a magnetic stirrer and transferred into a 100-mL stainless autoclave. The autoclave was placed in an oven at 100 °C for 150 min and the crystallized product was allowed to cool, and washed severally with distilled water until the pH of filtrate was 7. The sample was dried in an oven at 80 °C for 4 h. The reaction product was analyzed using XRD, SEM, and Brunauer–Emmett–Teller (BET) surface analysis.

### **Preparation of mango leaves extract**

The mango leaves collected were washed thoroughly with distilled water to remove dust from their surfaces before drying them under shade at room temperature for 18 d. After drying, they were crushed using a porcelain mortar and pestle. Around 20 g of crushed mango leaves was boiled in 200 mL of deionized water for 15 min. The mixture was allowed to cool and centrifuged at 6600 rpm for 30 min, it was decanted, filtered using Whatman filter paper. The filtrate was collected as the mango leaf extract and stored in a

bottle at a temperature of 4 °C for further experimental use. The phytochemical analysis was conducted on the extract to determine the phenolic, flavonoid, and tannin content in it.

### **Synthesis of silver nanoparticles**

A total of 0.017 g of  $\text{AgNO}_3$  was weighed with the aid of a digital balance and dissolved in 100 mL of deionized water to prepare 0.001 M. 9 mL of the 0.001 M of the salt prepared was put in a 50-mL conical flask and 1 mL of mango leaves extract was added to it. The silver nanoparticle was synthesized at a temperature of 30 °C and a reaction time of 15 min. At the end of 15 min, the sample was withdrawn for UV analysis after which the sample was freeze dried. The dried sample was analyzed using TEM.

### **Synthesis of zeolite doped silver nanoparticles (SDZA)**

A known mass (3.3 g) of synthesized zeolite A (SZA) was dispersed in 30 mL of deionized water and slowly stirred for 10 min to obtain a homogeneous mixture. In order to control the oxidation of silver during the reaction,  $\text{AgNO}_3$  was prepared in the dark bottle and 18 mL of the prepared 0.001 M  $\text{AgNO}_3$  was added to the zeolite A solution without direct sunlight during the reaction. The mixture was then stirred vigorously for a period of 30 min at room temperature before introducing 2 mL of mango leaf extract into it and stirred for another 15 min. The obtained mixture was centrifuged at 6000 rpm for 30 min, washed and dried in an oven for 2 h. It was then allowed to cool in air. The sample obtained was stored in dark bottle and characterized using BET (Qoantachrome NOVA 4200e), FT-IR (Perkin Elmer Frontier FT-IR), XRD (Bruker AXS D8), HRSEM (Zeiss Auriga T150T), and HRTEM (TECNAI G<sup>2</sup> F20-Twin) to determine the surface area, bind presence, crystallinity and surface morphology, respectively.

### **Collection and characterization of the textile wastewater (TWW)**

The TWW used in this study was collected from local textile industry in Ilorin, Kwara state,

Nigeria. The wastewater was analyzed based on the recommendation of standard methods of water and wastewater analysis at Regional Water Quality laboratory, Federal Ministry of Water Resources, Minna, Nigeria. The COD, BOD, TDS, alkalinity, the total amount of nitrate, nitrite, sulfate, phosphate, ammonium, chloride, cyanide and fluoride were determined by HACH instruments, USA using American Public Health Association (APHA, 2017) method. Other parameters investigated are Turbidity (Turbidity meter); pH (a multi-parameter analyzer C3010); electrical conductivity (a multi-parameter analyzer 2510B); and DO (dissolved oxygen meter).

### Adsorption studies

Batch adsorption study was employed in evaluating the rate and equilibrium data. Equilibrium isotherms were obtained by studying the adsorption process of SZA and silver doped zeolite A (SDZA) at different contact time, temperature, and adsorbent dosage. The effect of contact time was studied by varying the contact time of adsorbents with the textile effluent at 1, 3, 5, 10, 20, 30, 40, 50, 60, 90, 120, and 150 min in order to establish the adsorption equilibrium. Effects of temperature were studied at 30, 40, 50, and 60 °C so as to evaluate the adsorption thermodynamics parameters and effects of adsorbent dosage were also investigated from 0.5 to 2.0 g/100 mL at 0.5 g/100 mL intervals to investigate adsorption isotherms. All these were done on the TWW using SZA and SDZA at a temperature of 30 °C, except those studies in which the influence of temperatures were studied. The initial and final concentrations of the parameters studied in textile wastewater were done using HACH instruments for chloride, cyanide, BOD, COD, and nitrite, while the TOC content was determined by direct method.

Equilibrium adsorption of the textile effluent was performed by shaking 2 g of adsorbent in 100 mL of the textile effluent. This was placed in a shaker at a temperature of 30 °C and speed of 200 rpm for a period of 60 min. Adsorption equilibrium and percentage removal were calculated using the relationship as thus;

$$q_e = \frac{C_e - C_o}{m} x V \quad (2)$$

$$\% \text{ removal} = \frac{C_o - C_e}{C_o} x 100 \quad (3)$$

$q_e$  is the amount of adsorbate adsorbed at equilibrium (mg/g),  $C_o$ ; the initial adsorbate concentration in (mg/L),  $C_e$ ; the concentration of adsorbate at equilibrium (mg/L),  $m$  is the mass of adsorbent (g) and  $V$ ; the volume of the solution (mL).

### Adsorption isotherm

The adsorption isotherm models used to describe the adsorption processes in this study were Langmuir, Freundlich, Harkins–Jura and Jovanovic isotherm.

The Langmuir Isotherm is based on the postulation that there is formation of single layer of the adsorbate onto the exterior surface of the adsorbent, after which there will be no further adsorption. Hence, there is equilibrium distribution of the contaminants between the solid and the liquid phase (Langmuir, 1918; Turabik, 2008; Wang et al., 2014). This can be illustrated as:

$$q_e = \frac{q_m k_a C_e}{1 + k_a C_e} \quad (4)$$

The equation can be linearized in the form;

$$\frac{C_e}{q_e} = \frac{C_e}{q_m} + \frac{1}{K_a q_m} \quad (5)$$

where  $q_e$  is the quantity of contaminants adsorbed (mg/g),  $C_e$  is the equilibrium concentration of the adsorbate (mg/L),  $q_m$  and  $K_a$  are the Langmuir constant related to the maximum adsorption capacity (mg/g) and energy of adsorption (L/mg), respectively. The values of  $q_m$  and  $K_a$  can be estimated from the slope and intercept of plots of  $\frac{C_e}{q_e}$  against  $C_e$ . In addition, an imperative characteristic of the Langmuir isotherm can be stated with respect to dimensionless factor  $R_L$  (Hall et al., 1966), which is defined as;

$$R_L = \frac{1}{1 + b(C_o)} \quad (6)$$

The  $R_L$  value indicates the type of adsorption as unfavorable ( $R_L > 1$ ), linear ( $R_L = 1$ ), favorable ( $0 < R_L < 1$ ) or irreversible ( $R_L = 0$ ).  $R_L$  is the dimensionless constant separation factor,  $b$ ; the Langmuir adsorption constant related to the affinity of the binding sites in L/mg,  $C_o$ ; the liquid-phase initial concentration of contaminants in mg/L. The Freundlich Isotherm is basically used to



describe the binding of adsorbates onto heterogeneous surfaces as well as the adsorption of many layers and it is expressed as;

$$q_e = k_f C_e^{1/n} \quad (7)$$

and can be linearized in the form;

$$\log q_e = \log K_f + \frac{1}{n} \log C_e \quad (8)$$

where  $q_e$  is the amount adsorbed at equilibrium (mg/g),  $K_f$  is the Freundlich constant,  $1/n$  is the heterogeneity factor,  $K_f$  and  $1/n$  are linked to the capacity and the intensity of the adsorbent,  $C_e$  is the equilibrium concentration (mg/L). The values of  $K_f$  and  $1/n$  can be obtained from the slope and intercept of the plot of  $\log q_e$  vs.  $\log C_e$  (Freundlich, 1906). The Harkin–Jura Isothermal Model is based on the assumption that there is monolayer adsorption on an adsorbent that has heterogeneous pore distribution (Ayawei et al., 2017), which is linearly expressed as;

$$\frac{1}{q_e} = \frac{B}{A} - \frac{1}{A} \log C_e \quad (9)$$

$B$  and  $A$  are the Harkin–Jura isotherm constants which are evaluated from the slope and intercept of plots of  $1/q_e$  against  $\log C_e$ . The Jovanovic Isotherm follows the assumption by Langmuir except that it explores the prospect of some mechanical interactions between the adsorbing and the desorbing molecules. Its non-linear expression is in the form presented in Equation (10) (Markovic et al., 2014);

$$q_e = q_j (1 - \exp(-k_j C_e)) \quad (10)$$

and its linear form is;

$$\ln q_e = \ln q_j - k_j C_e \quad (11)$$

where  $q_j$  and  $k_j$  are the constants evaluated from the slopes and intercepts of the plots of  $\ln q_e$  vs.  $C_e$ .

### Adsorption kinetics

The adsorption kinetics study is vital as it determines the effectiveness of the adsorption in relation to the quantity of contaminants adsorbed at equilibrium with respect to the time of contacts. It also examines the mechanism of adsorption and rate-controlling steps of the reactions. The adsorption mechanisms of chemical parameters onto synthesized zeolites were investigated using

Lagergren pseudo-first order kinetics, pseudo-second order and the intraparticle diffusion model. The Lagergren pseudo-first order model was tested in this work using the Lagergren pseudo-first order kinetics linear equation as expressed in Equation (12);

$$\log(q_e - q_t) = \frac{1}{q_e} - \frac{k_1}{2.303} t \quad (12)$$

$k_1$  is the pseudo-first order rate constant in ( $\text{min}^{-1}$ ). If a Pseudo-first order model applies, then a reversible reaction occurs in the process which is recognized by the existence of equilibrium between the contaminants and the adsorbents (Radnia et al., 2011). The pseudo-second order equation is generally expressed linearly as (Yakout et al., 2010);

$$\frac{t}{q_t} = \frac{1}{k_2 q_e^2} + \frac{1}{q_e} t \quad (13)$$

$q_e$  and  $q_t$  are the amounts of adsorbates adsorbed at equilibrium and time ( $t$ ), respectively,  $k_2$  and  $r_i$  are the pseudo-second order constant in ( $\text{g}/\text{mg}\cdot\text{min}$ ) and ( $\text{mg}/\text{g}\cdot\text{min}$ ) accordingly, where;

$$r_i = k_2 q_e^2 \quad (14)$$

If the pseudo-second model applies, a straight-line graph through which the slopes and intercept evaluated from it gives the constants, and then chemisorption is the rate-limiting step of the sorption process (Radnia et al., 2011). The intraparticle diffusion model developed by Morris and Webber (Yakout et al., 2010) is linearly expressed as;

$$q_t = k_m \cdot t^{0.5} + C \quad (15)$$

where  $k_m$  is the rate constant in ( $\text{mg}/\text{g}\cdot\text{min}^{0.5}$ ) and  $C$  is another constant related to the thickness of the boundary layer in ( $\text{mg}/\text{g}$ ). If the plots of  $q_t$  vs.  $t^{0.5}$  produce a straight line through the origin, then the adsorption is controlled by intraparticle diffusion only; if it does not pass through the origin then; intraparticle diffusion is involved. However, if multilinear occur, then more kinetic models are associated with the transport of the adsorbates onto the adsorbent surface (Fierro et al., 2008; Yakout et al., 2010).

### Thermodynamics of adsorption

The spontaneity of the sorption of the adsorbate–adsorbents can be accessed through thermodynamic parameters such as enthalpy change ( $\Delta H^\circ$ ), Gibb's free energy ( $\Delta G^\circ$ ) and entropy change ( $\Delta S^\circ$ ). Any reaction where ( $\Delta H^\circ$ ) and ( $\Delta G^\circ$ ) are negative, whereas ( $\Delta S^\circ$ ) is positive, implies a spontaneous reaction (Margeta et al., 2013). Thus;

$$\Delta G^\circ = \Delta H^\circ - T\Delta S^\circ \quad (16)$$

$$\ln K = \frac{\Delta S^\circ}{R} - \frac{\Delta H^\circ}{RT} \quad (17)$$

$\Delta H^\circ$  and  $\Delta S^\circ$  are evaluated from the slope and intercept of the plot of  $\ln K$  vs.  $1/T$  and the free energy of specific adsorption  $\Delta G^\circ$  ( $\frac{kJ}{mol}$ ) can be calculated using Equation (16).

### Results and discussions

#### Characterization of the synthesized zeolites

The elemental composition of the raw, refined and metakaolin produced from Nigerian Ahoko

**Table 1.** Elemental composition of raw AH, refined AH kaolin and metakaolin.

Oxides	Raw kaolin (%)	Refined kaolin (%)	Metakaolin (%)
SiO <sub>2</sub>	62.25	58.83	54.30
Al <sub>2</sub> O <sub>3</sub>	22.57	26.36	36.11
MgO	0.15	0.15	0.16
Na <sub>2</sub> O	0.02	0.01	0.01
P <sub>2</sub> O <sub>5</sub>	0.12	0.11	0.12
K <sub>2</sub> O	1.01	0.95	0.96
CaO	0.04	0.05	0.09
TiO <sub>2</sub>	2.49	2.41	0.22
V <sub>2</sub> O <sub>5</sub>	0.03	0.03	2.64
Cr <sub>2</sub> O <sub>3</sub>	0.01	0.01	0.01
MnO	0.02	0.02	0.02
Fe <sub>2</sub> O <sub>3</sub>	2.66	2.14	2.21
LOI	8.59	9.11	3.45
Total	100	100	100
SiO <sub>2</sub> /Al <sub>2</sub> O <sub>3</sub>	2.76	2.23	1.50

kaolin is presented in Table 1. The results revealed the presence of SiO<sub>2</sub> and Al<sub>2</sub>O<sub>3</sub> as the main constituents. It further shows reduction in SiO<sub>2</sub> content and an incremental in Al<sub>2</sub>O<sub>3</sub> of the raw, refined and metakaolin, respectively. The percentage of SiO<sub>2</sub> decreased from 58.83% to 54.30% and Al<sub>2</sub>O<sub>3</sub> increased from 26.36% to 36.11% for refined and metakaolin, respectively. The reduction in SiO<sub>2</sub> after refining suggest reduction in quartz content which is an impurity and as such needed to be reduced in applications such as zeolite synthesis (Kovo, 2011, 2012). This is because silica is known to be associated with quartz, which settled down during the refining process because of its density which is higher than that of kaolinite, hence, some of it was not collected with the kaolin which resulted to reduction in the silica content as observed in the Table 1. Hence, there was reduction in quartz content and the kaolinite was enriched. The SiO<sub>2</sub>/Al<sub>2</sub>O<sub>3</sub> ratio for the metakaolin was calculated to be 1.5 which favors the synthesis of zeolites A, as higher SiO<sub>2</sub>/Al<sub>2</sub>O<sub>3</sub> > 5 tend to reduce their crystallinity (Cejka et al., 2007; Mirfendereski and Mohammed, 2016).

The XRD pattern of the refined and metakaolin are shown in Figure 1 while that of SZA and silver doped zeolite A in Figure 2. The result shows that the main peaks at  $2\theta = 12.24^\circ$  and  $24.76^\circ$  which were the main peaks in identifying kaolinite in refined kaolin (Figure 1) were no longer observed in the metakaolin diffraction pattern. This is because kaolin has been transformed to a more reactive phase of metakaolin due to breakdown in its crystal lattices by heat, which

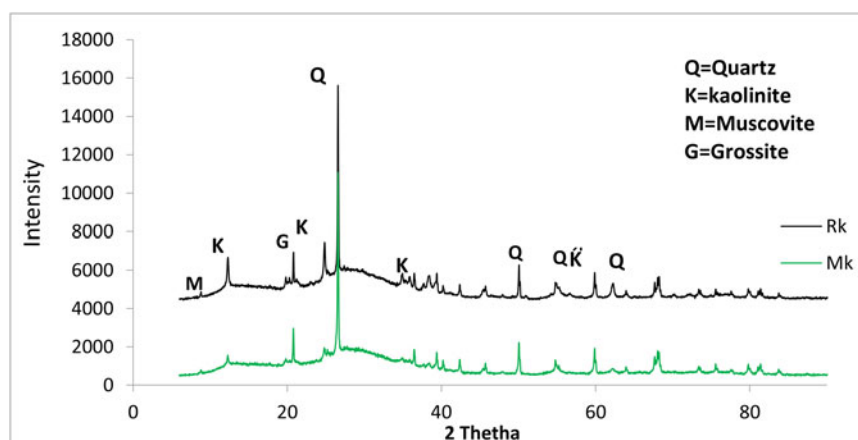


**Figure 1.** XRD pattern of refined and Metakaolin.

has led to the formation of an amorphous and disordered structure (Said-Mansour et al., 2011; Johnson et al., 2014). Thus, the predominant phase that appeared as the crystalline phase is quartz with minor impurities of muscovite and grossite. This is in line with previous work reported by Gougazeh and Buhl (2010, 2014) and Zhao *et al.* (2004).

The UV spectra obtained for biosynthesis of AgNPs is shown in Figure 3. A color change from light yellow to dark brown was observed at the completion of 15-min reaction time, which is an indication of formation of silver nanoparticles (Song and Kim, 2009). This was confirmed using UV-Vis spectroscopy analysis which showed a corresponding wavelength at 431.50 nm as presented in Figure 3. Hence, the color change was due to the excitation of the Surface Plasmon Vibrations (Song and Kim, 2009; Shah et al., 2014) as a result of reduction of the silver salts

by the mango leaf extract to form silver nanoparticles (AgNPs); Similar results were obtained in the literature (Sarsar et al., 2013; Sekhar et al., 2016; Shakeel Ahmed et al., 2016; Sivashanmugam, 2017).

The morphology and size distribution of the synthesized AgNPs was investigated using TEM analysis as shown in Figure 3(b). Well defined cubic shapes of AgNPs which are evenly distributed were obtained. This is an indication that after the mono valence of the silver salt has been reduced to a zero valent state by the mango leaf extract, nucleation proceeds and the smaller particles of AgNPs aggregate to form larger nanoparticles which are more thermodynamically stable. Thus, as the growth progresses the AgNPs aggregate to form a cubic morphology at 15 min.

The XRD pattern of SZA and silver nanoparticle doped zeolite A (SDZA) are shown in Figure 2. The result shows reflections at  $7.1^\circ$ ,  $10.10^\circ$ ,  $12.4^\circ$ ,  $16.0^\circ$ ,  $21.6^\circ$ ,  $24^\circ$ ,  $26.3^\circ$ ,  $29.8^\circ$ ,  $30.7^\circ$ ,  $32.5^\circ$ , and  $34.1^\circ$  two-theta; which are the main peaks in identifying zeolite A (Zhao et al., 2004). Also, the XRD pattern of SDZA shows a reduction in the intensity of peaks at  $38.10^\circ$ ,  $43.45^\circ$ , and  $58.55^\circ$ , and  $63.32^\circ$ . This is a suggestion that the incorporation of the silver nanoparticles into the SZA framework, has led to a reduction in the intensity of these peaks. These results are in good agreement with literature (Kamyar et al., 2011; Odutayo et al., 2016).

The morphology of the SZA and SDZA as revealed by SEM and TEM micrographs are shown in Figure 4. Figure 4(a) shows perfect

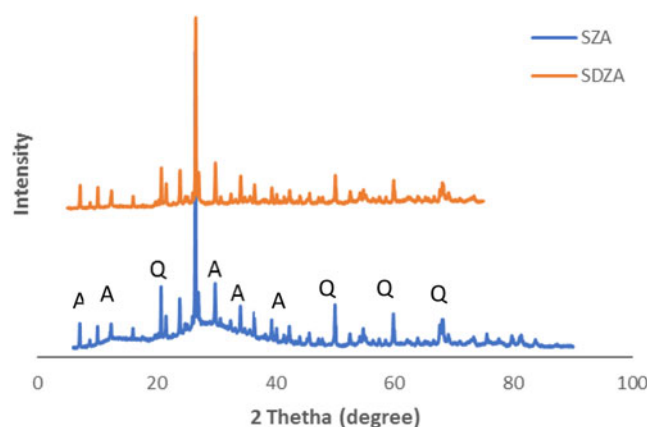


Figure 2. XRD pattern of SZA and SDZA.

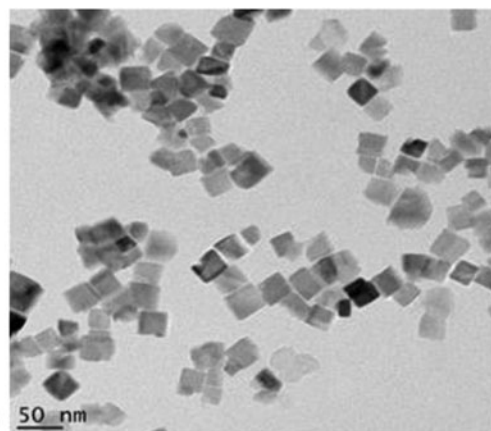
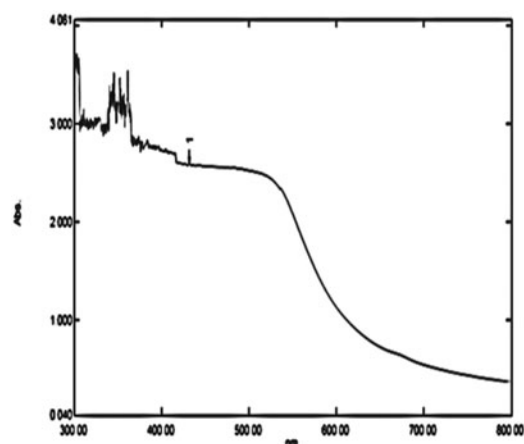
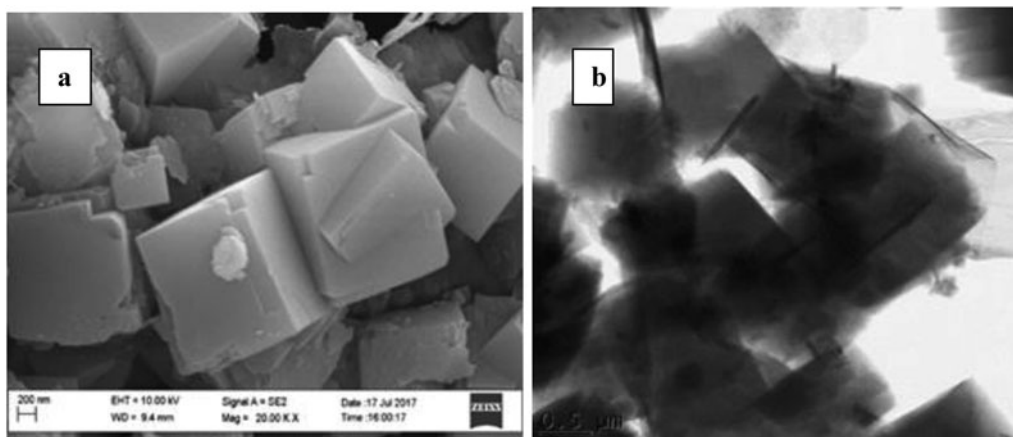


Figure 3. (a) UV-Vis spectroscopy of synthesized AgNPs; (b) TEM image of AgNPs.





**Figure 4.** SEM image of SZA (a) and TEM image of SDZA.

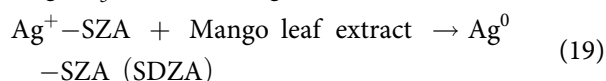
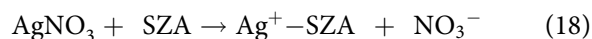
**Table 2.** BET analysis of synthesized adsorbents.

	SZA	SDZA
BET surface area (m <sup>2</sup> /g)	119.98	436.44
Pore diameter (nm)	3.328	5.90
Total pore volume (cc/g)	0.039	0.173

cubic crystals with sharp edges depicting the well-defined cubic crystalline phase of zeolite A which is in good agreement with XRD result and the TEM micrographs, revealing that the AgNPs are well dispersed on the cubic shape of SZA as shown by the cubic patches on its surface. The cubic patches suggest the cubic nature of AgNPs which is expected to increase the porosity of the SZA.

In order to assess the effect of doping on the surface area of the SZA, BET analysis was conducted. The results as shown in Table 2 show that the surface area and pore diameter of the SZA increased from 119.98 m<sup>2</sup>/g to 436.44 m<sup>2</sup>/g and 3.328 nm to 5.90 nm, respectively. The expanded surface area might be due to non-clogging of the zeolite channel after the incorporation of silver nanoparticle into its framework. As illustrated in Equation (18), when silver nitrate reacts with the SZA, there was increase in the pore volume due to the low concentration of silver nitrate used, this consequently resulted to lower exchanged in Ag-SZA since higher concentration will result to higher exchange which will subsequently reduce the pore volume. However, when the mango leaf extract was added as illustrated in Equation (19), there was reduction of the silver ion to silver nanoparticles, this tend to increase the aperture size of the SZA, thus, increased the

accessible path of N<sub>2</sub> molecules used during the textural characterization. This in turn increased the accessibility of the silver nanoparticles into the channels of SZA, bringing about high specific surface area as observed in the present study. Also, SDZA with higher pore diameter and total pore volume implies a higher porosity and number of pores, respectively (Zainal Abidin et al., 2017).



The FTIR of SZA and SDZA were performed to study the effect of the synthesized nanoparticles on the surface of SZA as shown in Figure 4. The IR spectrum of SZA (Figure 5(a)) reveals bands at 3695–3622 cm<sup>-1</sup> which is attributed to the hydrogen group of water molecules present in the pores of zeolite A, while that at 1658 cm<sup>-1</sup> with the sharp and low intensity bands corresponding to the bending vibration of water. The sharp peak around 1000 cm<sup>-1</sup> corresponds to the asymmetric stretching vibrations of all zeolitic materials (Byrappa and Suresh Kumar, 2007; Sarsar et al., 2013). The absorption band at 692 cm<sup>-1</sup> is associated with symmetric stretching of T-O-T vibrations of LTA framework which is in good agreement with 693 cm<sup>-1</sup> reported by Gougazeh and Buhl (2014) for D4R zeolite group. The spectrum at 774 cm<sup>-1</sup> was due to the external linkage tetrahedral regions of the D4R units (Byrappa and Suresh Kumar, 2007).

The spectra of the SDZA as revealed in Figure 5(b) shows the same spectra pattern with SZA

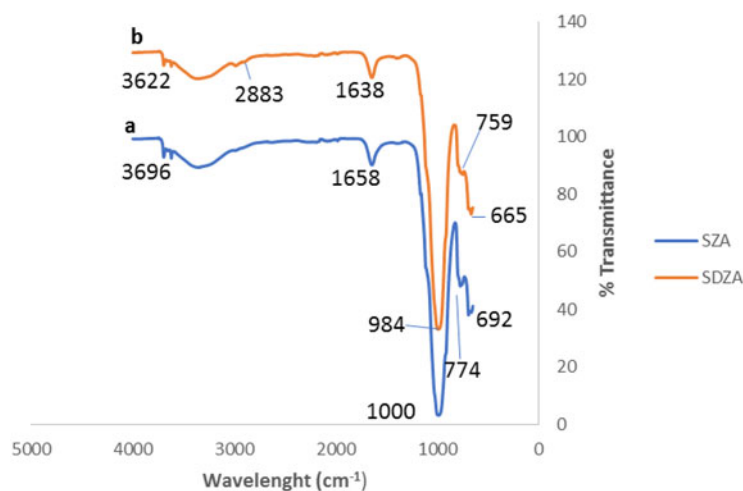


**Figure 5.** FTIR of SZA and SDZA.

(Figure 5(a)) except for the additional band noticed at  $2883\text{ cm}^{-1}$ . This is attributed to the carboxyl group present on the surface of the nanoparticles. In addition, the decrease in the intensities of peaks of the SDZA in Figure 5(b) as compared to SZA in Figure 5(a) indicated the successful doping of the nanoparticles in the framework of the zeolite A. This result further supports the XRD results which showed reduction in the intensities of the peaks of doped zeolites as compared to SZA.

#### **Physicochemical parameters of textile wastewater**

Determination of physicochemical parameters is very crucial in maintaining good water quality for drinking, domestic and other purposes (Elango et al., 2017). It also serves as a guide in launching tactics of controlling oxygen depletion by having low BOD and COD in the water bodies. The physicochemical parameters of the textile effluent were analyzed and the results (before and after treatments with SZA and SDZA) with their various permissible limits/standards based on World Health Organization/Environmental Protection Agency (WHO/EPA) and Nigerian Industrial Standards (NIS) are presented in the Table 3.

According to Table 3, the pH of the textile effluent was 11.2 before treatment and 9.7 and 9.35 after treatment with SZA and SDZA, respectively. This suggests that the water was highly toxic as the toxicity of water increases with pH and the pollution may be due to strong

bases such as sodium hydroxide or calcium hydroxide employed during dyeing and coloring operation of the fabrics (Elango et al., 2017). Extremely high or low pHs have drastic effect on living creatures, extremely high pH in water which results in the death of fishes, due to damage to their vital organs such as the gills, eyes, and skin. This can also lead to the inability to dispose metabolic waste by the fishes (Odutayo et al., 2016). In addition, high pH above 11 and low pH below 4 can result in skin and eye irritation in human (Weber-Scannell and Duffy, 2007). The values obtained after treatment compare well with the EPA standards for SDZA except for SZA which needs further neutralization with base to maintain the water quality. The total alkalinity of the wastewater was  $12,750\text{ mg/L}$  as indicated in Table 3 which decreased to the range of  $400\text{--}450\text{ mg/L}$  after treatment. The value of SDZA is in line with EPA standard while that of SZA did not.

The physical parameter examined as shown in the table is turbidity and the value reduced from  $7500\text{ NTU}$  to  $85\text{--}89\text{ NTU}$ . Though, the values do not conform to all the standards, nevertheless, there was drastic reduction in the value. It is also worthwhile to mention that the rate of removal solely depends on the initial concentration of the adsorbate/contaminant present in the effluent (Margeta et al., 2013).

The TDS of the raw textile effluent was found to be  $36,582\text{ mg/L}$  which is very high. However, the concentration dropped to  $804\text{ mg/L}$  and

6-  
3-  
7-**Table 3.** Physicochemical parameters of textile effluent and their various standards using adsorbent dosage of 2 g/100 mL of wastewater.

Physicochemical parameters	Conc. Before treatment	Concentrations after treatment with SZA	Concentrations after treatment with SDZA	Standard limits (WHO/EPA)	Standard limits (NIS)
pH	11.2	9.70	9.35	6.5–8.5/6.5–9.5	6.5–8.5
TDS (mg/L)	36,582	804	637	1000/-	500
Conductivity ( $\mu S/cm$ )	54,600	1200	950	-/1000–2500	1000
Dissolved oxygen (mg/L)	2.80	3.10	3.50	-	-
Turbidity (NTU)	7,500	89	85	1.5/1.0	5.0
Total alkalinity (mg/L)	12,750	450	400	-/400	-
Nitrate (mg/L)	1300	25.9	23.1	50/50	50
Ammonium (mg/L)	250	5.10	4.40	1.3–3.5/0.2–4.0	-
Chloride (mg/L)	9,221	132	39.0	250/250	250
Phosphate (mg/L)	105	1.50	1.25	-/0.5–0.7	-
Cyanide (mg/L)	6.70	0.04	0.01	-/0.05	0.01
Fluoride (mg/L)	160	8.20	7.10	1.5/1–1.7	1.5
Sulfate (mg/L)	7,000	33	27	500/250	100
COD (mg/L)	30,083	71	60.0	-/40	-
BOD (mg/L)	6,016	4.80	2.79	-	5.0
TOC (mg/L)	2,110	360	440	-	-
Carbonate (mg/L)	300	25	23	-	-
Nitrite (mg/L)	13.7	0.42	0.09	3.0/0.5	0.2

Note: World Health Organization (WHO, 2011), Environmental Protection Agency (EPA, 2001) and Nigerian Industrial Standards (NIS, 2007).

mg/L when treated with SZA and SDZA, respectively. These results compare well with the limits suggested by WHO of 1000 mg/L. The high concentration of TDS present in the raw effluent could be as a result of the effluent being highly colored due to different types of dyes used during the coloring operations (Varsha and Singh Seema, 2013; Tafesse et al., 2015; Elango et al., 2017). Very high or too low TDS beyond permissible limits can limit the growth of aquatic organisms or even results to death. High TDS water often results to high hardness and tastes bad to human (Sherrard et al., 1987; Weber-Scannell and Duffy, 2007). The electrical conductivity (EC) was 54,600  $\mu S/cm$  which reduced to the range of 950–1200  $\mu S/cm$  after treatments. These results correlated well with literature as TDS was correlated to be 0.55–0.7 of EC, while the high concentration of EC is attributed to high dissolved ions in the water sample (Thiruvengkatahari et al., 2008). Thus, the reduction in the electrical conductivity is a result of reduced dissolved ions in the water.

Other chemical inorganic parameters shown in the table are nitrate, nitrite, ammonium, phosphate, cyanide, chloride, fluoride and sulfate. The value of nitrate, nitrite and ammonium are 1300 mg/L, 13.7 mg/L and 250 mg/L before treatment, these were reduced to the range of 23.1–25.9 mg/L, 0.09–0.42 mg/L and 4.40–5.10 mg/L after treatments with the synthesized adsorbents accordingly. It can be observed from the results that the nitrite has the lowest concentration which is not unusual as nitrogen in effluent have the habit of existing in the form of ammonia/ammonium ion or nitrates (EPA, 2001) and nitrite is an intermediary in formation of nitrates from ammonia. Nitrites can poison the fish's blood through their circulatory system at high level, thereby turning their blood to brownish color; they also impair the blood hemoglobin in human by rendering the blood cells inefficient for transportation of oxygen in which babies less than 3 months are most affected (Sivakumar et al., 2011).

The level of chloride and cyanide in the sample were 9221 and 6.70 mg/L which decreased to 39–132 mg/L and 0.01–0.04 mg/L, respectively, after treatments. The high content of chlorides

in the sample may be as a result of compounds such as hydrochloric acid, hypochlorous acid and chlorine gas used in different processes such as bleaching, washing and disinfection of the material (Elango et al., 2017). This has drastic effect on the aquatic life as it can destroy microorganisms required to maintain the food chains (Varma and Sharma, 2011). Nevertheless, their values after contact with the developed adsorbents conform well to all the standards, suggesting that the treated water can be used for drinking and other purposes (NIS, 2007; Thiruvengkatachari et al., 2008; WHO, 2011).

The organic contents of the textile wastewater were also examined as presented in Table 3 through their investigations with respect to DO, COD, BOD and TOC analyses. The DO was 2.80 mg/L in the sample which was brought to the range of 3.10–3.50 mg/L after contacts with the adsorbents. This shows that treatment with synthesized adsorbents has raised the level of oxygen required by the bacteria for their aerobic activities. It is also important to mention that shallow water fish cannot survive in the water treated in this work as they require high levels of DO (4–15 mg/L) but bottom feeders, crabs, oyster and worms can comfortably survive, since this class require minimal DO of 1–6 mg/L (Fondriest Environmental Inc, 2013). The COD, BOD, and TOC of the collected sample were found to be 30,083, 6,016, and 2110 mg/L which were drastically reduced to 60–71, 2.79–4.80, and 160–440 mg/L, respectively. The COD measures the DO required for oxidation of all organic matter into carbon dioxide and water in the sample. The treated water did not meet the required water standard of 40 mg/L set by EPA for COD, however 99.76–99.80% treatments were achieved. The BOD level conformed to the standard suggested by EPA as WHO/NIS did not see it as a factor of concern in drinking water. The high level of BOD and COD in the raw sample is an indication of inadequate oxygen for living organisms in water, thereby posing threat to human life and the environment (Dey and Islam, 2015; Tafesse et al., 2015). These parameters are highly important in water treatment because they serve as an indicator, so; the analysis is required from time to time (Thiruvengkatachari et al., 2008).

Furthermore, sulfate and fluoride content were also determined to be 7000 and 160 mg/L which were further reduced to, 27–33 mg/L and 7.10–8.20 mg/L, respectively, after treatments. The carbonate concentrations were 300 mg/L and 23–25 mg/L before and after treatments, respectively. The result suggests that the treatment of the effluent lead to the production of soft water using the developed adsorbents. This is in accordance with EPA, who classified water with carbonate content of 251–350 mg/L as hard water and up to 50 mg/L as soft water (EPA, 2001). Therefore, the water can be conveniently used for domestic application. These results show that the synthesized adsorbents can effectively be used in treatment of textile wastewater.

#### *Effects of contact time on adsorption studies of chemical parameters in textile effluent*

The results of the effect of contact time on the removal of chemical parameters (chloride, cyanide, COD, BOD, nitrite, and TOC) by the SZA and the doped zeolite A(SDZA) are as shown in the Figure 6.

The figures show that the removal of chemical parameters of textile effluents increased progressively with contact time in both adsorbents until they both reached equilibrium at 60 min except for the removal of TOC by the SDZA which got to equilibrium at 20 min. It is also evident from the results presented that there was rapid removal of the contaminants within the first minute of contacts with the adsorbents, removing 82.94–99.81% and 92.42–99.90% for SZA and SDZA, respectively. This is attributed to the higher number of active sites initially present at the surface of the adsorbents leading to attraction of the contaminants onto their surfaces, respectively. Furthermore, the percentage removal was higher with SDZA than SZA due to the higher surface area and porosity possessed by it, showing the effectiveness of doping and improvement in the SZA surface property, consequently; leading to the increase in adsorption capacity. The progressive increment in the degradation of contaminant until equilibrium before gradual decrement implies that the surface of the adsorbents became saturated and therefore could not adsorb



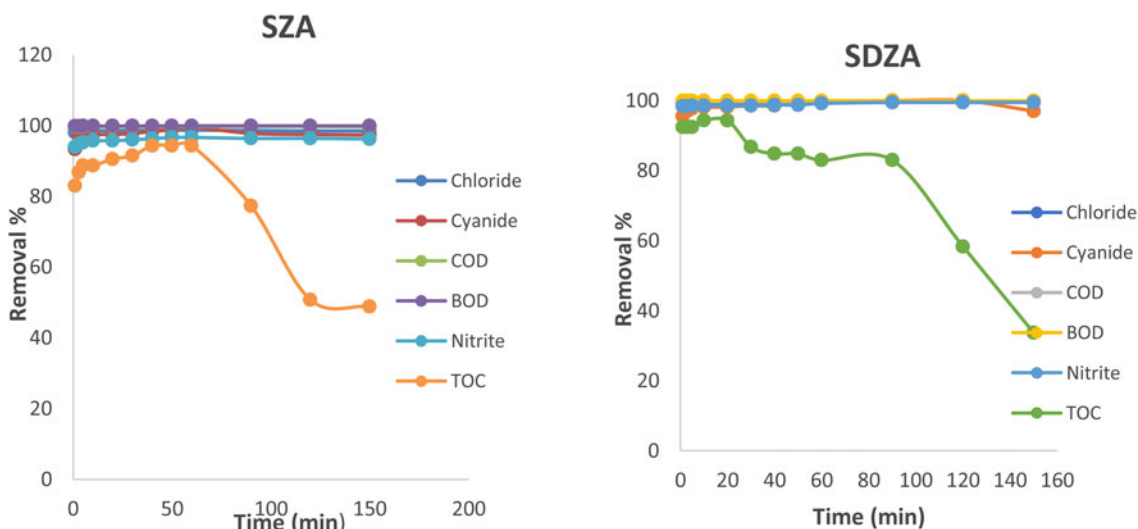


**Figure 6.** Effect of contact time on removal of chemical parameters onto (a) SZA and (b) SDZA (temperature =30 °C, speed = 200 rpm and adsorbent dosage= 1.0 g/50 mL).

much of the contaminants. Consequently, there was fall in the percentage removal of the contaminants as shown in the presented results. Array of removal is in the following; BOD > COD > CN<sup>-</sup> > Cl<sup>-</sup> > NO<sub>2</sub><sup>-</sup> > TOC for SZA and CN<sup>-</sup> > BOD > COD > NO<sub>2</sub><sup>-</sup> > Cl<sup>-</sup> > TOC for the doped adsorbent. It is expected that the percentage removal of nitrite will be greater than cyanide according to the rule of ionic radius (ionic radius of NO<sub>2</sub><sup>-</sup> =155 rpm, CN<sup>-</sup> =177 rpm and Cl<sup>-</sup> =184 rpm), however, it should be noted that the rate of adsorption cannot solely be dependent on the ionic radius as the initial concentration of the contaminant present in the waste water also play a vital role. As such, in the present study, cyanide has the minimum concentration which might be responsible for its higher removal.

#### **Effects of sorbent dose on adsorption studies of chemical parameters in textile effluent**

The quantity of the adsorbent used in adsorption studies has been identified as an important factor which determines the rate at which contaminant are attached on the surface of sorbents (Desta, 2013; Margeta et al., 2013). This parameter was analyzed in the present study at different dosages of 0.5–2.0 g/100 mL at 30 °C for 60 min which was identified as a specific period at which there will be maximum sorption of the contaminants. The results are shown in the Figures 7(a) and 7(b) for SZA and SDZA, respectively.

The figures show that sorption of the contaminants onto the surface of developed adsorbents increased as the quantity of the SZA and SDZA increased. For instance, the percentage removal of cyanide increased from 95.31 to 99.56% for SZA and from 96.00 to 99.98% for SDZA, while that of TOC are 67–82.9% and 77–88.9% by SZA and SDZA, respectively, when the quantity of the adsorbents was increased from 0.5 to 2.0 g. They all still follow the previous array of removal which is BOD > COD > CN<sup>-</sup> > Cl<sup>-</sup> > NO<sub>2</sub><sup>-</sup> > TOC for SZA and CN<sup>-</sup> > BOD > COD > NO<sub>2</sub><sup>-</sup> > Cl<sup>-</sup> > TOC for the doped sample. The increments in the percentage removal of the contaminants were due to the increase in the active/sorption sites of the zeolite A (ZA) surface. This subsequently increases the amount of the contaminants adsorbed. This suggests that the sorption sites increased with increase in the quantity of the adsorbent. The results obtained in this work is in line with those found in the literature (Al-Anber, 2011; Margeta et al., 2013; Yusuf-Alaya, 2014; Bankole et al., 2017). However, the removal of TOC by these adsorbents were noticed to be the lower than other pollutants, this might be due to some its molecules been too large to pass through the pores of the developed adsorbents, as it can be noticed that the SDZA with larger pore size removed TOC better than SZA (Mates et al., 2004).



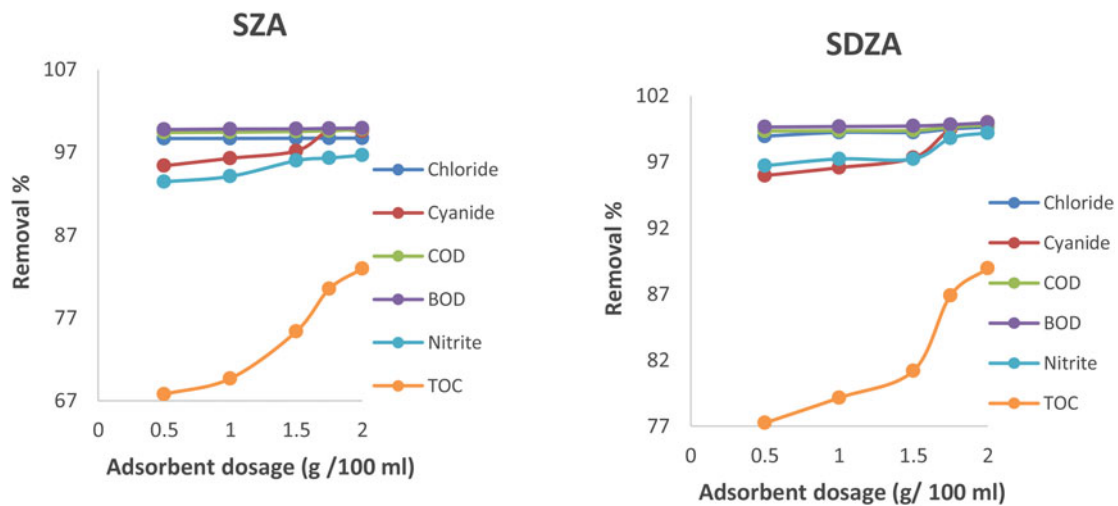


**Figure 7.** Effect of sorbent dose on removal of chemical parameters onto (a) SZA and (b) SDZA (temperature = 30 °C, speed = 200 rpm and stirring time = 60 min).

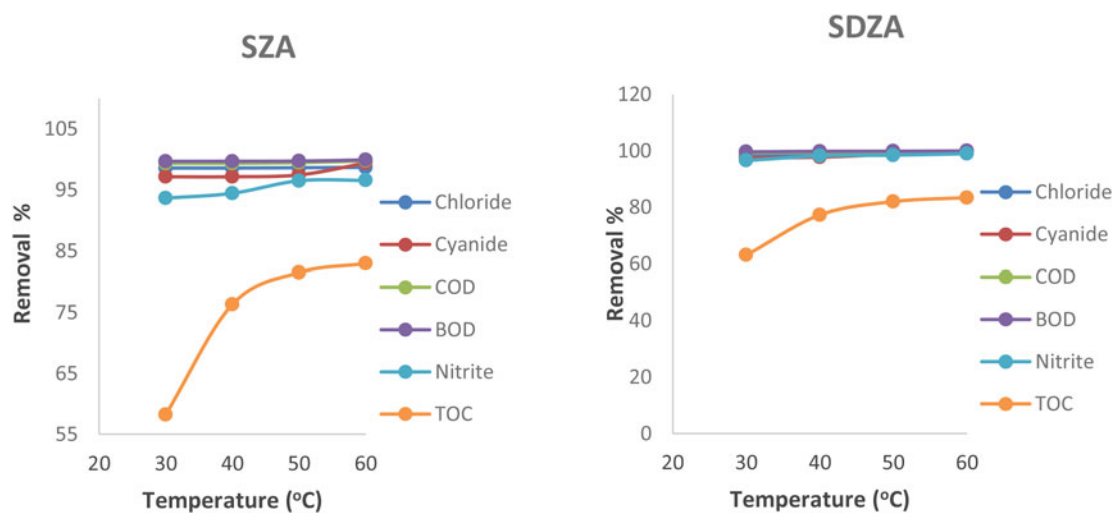


**Figure 8.** Effect of temperature on removal of chemical parameters onto (a) SZA and (b) SDZA (stirring time = 60 min, stirring speed = 200 rpm and adsorbent dosage = 1.0 g/50 mL).

### **Effects of temperature on adsorption studies of chemical parameters in textile effluent**

Temperature is an important parameter to be studied in adsorption processes, as the type of reaction and the mechanism taken place in the adsorption can be assessed (Al-Anber, 2011). Adsorption can be physical or chemical depending on the type of attraction binding the adsorbate onto the adsorbent. The effects of temperature on degradation of contaminants were studied on the developed adsorbents by varying the temperatures from 30 to 60 °C while keeping other parameters constant; stirring time of 60 min, stirring speed of 200 rpm and

adsorbent dosage of 1.0 g/50 mL. The results obtained are presented in Figure 8.

The figures revealed that the adsorption rate of the chemical parameters increased with increase in temperature in all cases. This is attributed to immobility of the chemical parameters molecules as the temperature increased, which subsequently; resulted to formation of strong binding force between the contaminants and the zeolites A (Acemioglu, 2010; Al-Anber, 2011; Yusuf-Alaya, 2014; Bankole et al., 2017). Hence, the type of adsorption taking place can be described as chemisorption process (Al-Anber, 2011).

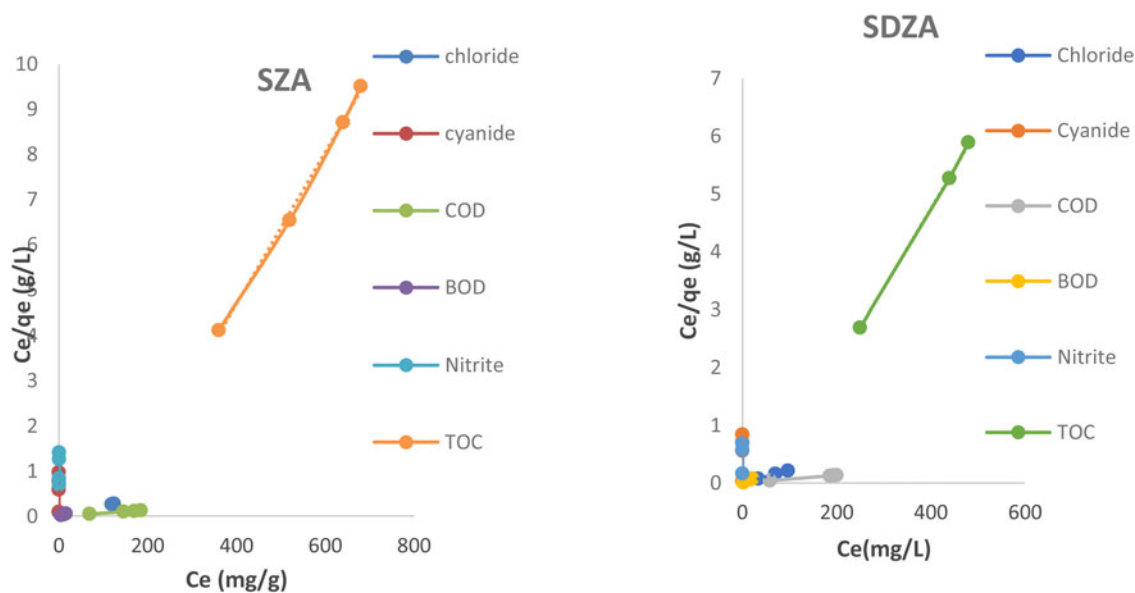


Figure 9. Langmuir plots of chemical parameters onto SZA and SDZA.

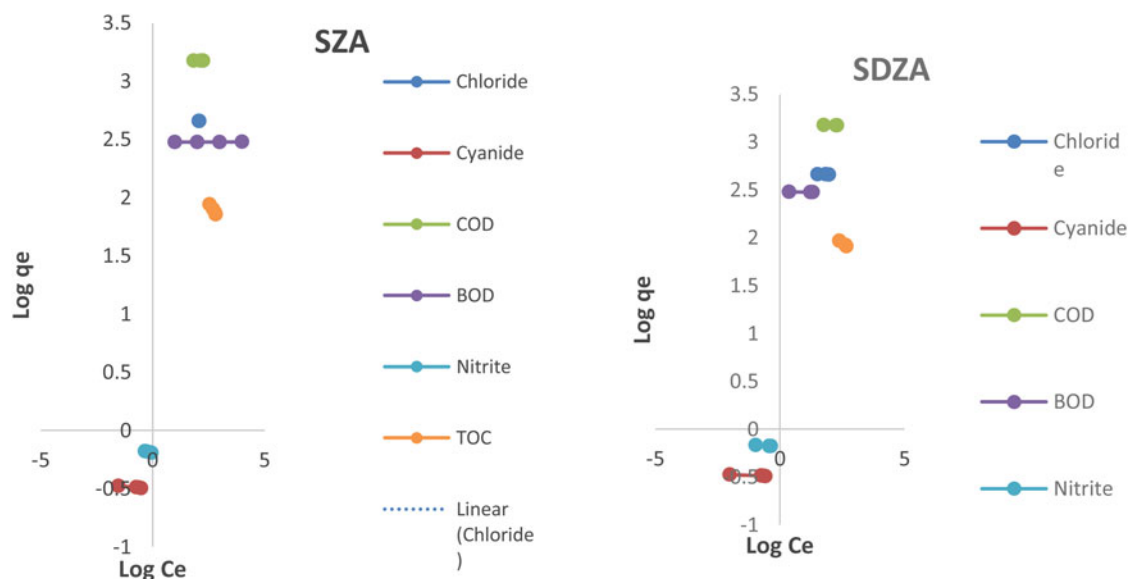


Figure 10. Freundlich plots of chemical parameters onto SZA and SDZA.

### Adsorption isotherms

The Langmuir model (Equation (5)), Freundlich model (Equation (8)), Harkins–Jura model (Equation (9)) and Jovanovic model (Equation (11)) were used in establishing the best isotherm model to describe the adsorption processes in this work as illustrated in Figures 9–12.

The Langmuir isotherm is based on the assumption that the adsorption process takes place at an exact single layer of the adsorbent, after which, there will be no further adsorption. The Langmuir plots are shown in Figure 9 and the parameters are

presented in Tables 4 and 5, respectively, for zeolite A and silver nanoparticle doped zeolite A adsorbents. Maximum adsorption capacity ( $q_m$ ) of the adsorbents (SZA and SDZA) as presented in the tables for chloride, cyanide, COD and BOD are 454.55 mg/g, 0.32 mg/g, 1,428.57 mg/g and 303.03 mg/g, respectively. This shows that the adsorbents have the same affinity for these contaminants. Even though, SDZA (Table 5) has higher capacity of 0.66 mg/g and 72.46 mg/g for nitrite and TOC, respectively; as compared to SZA (0.62 mg/L for nitrite and 59.52 mg/L for TOC as

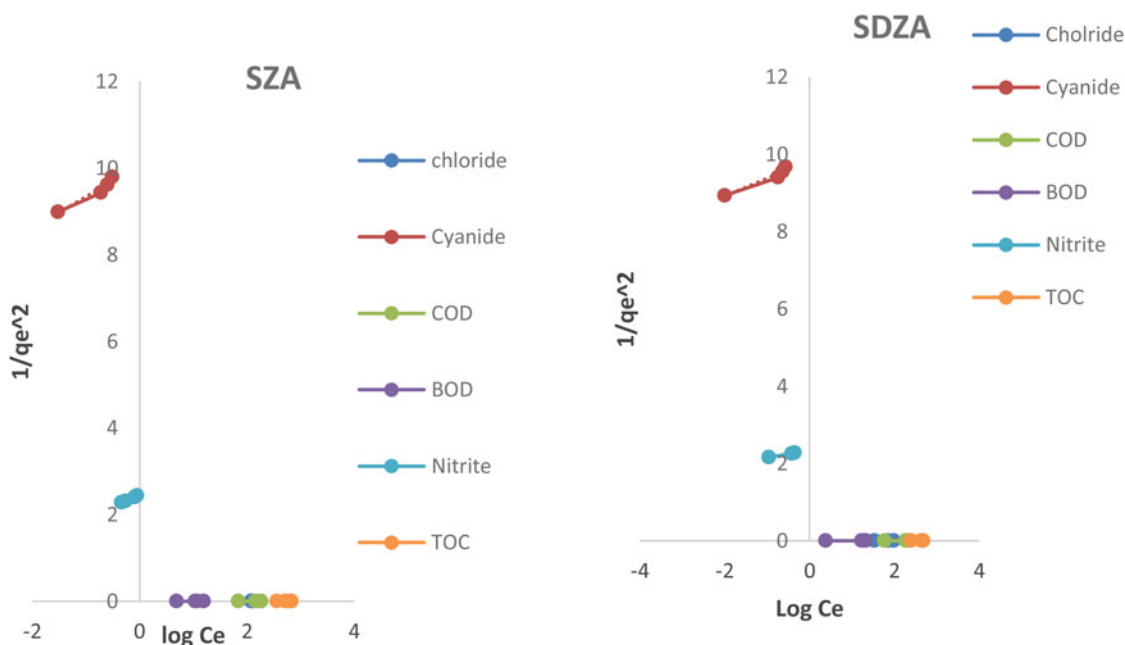


Figure 11. Harkins–Jura Plots of chemical parameters onto SZA and SDZA.

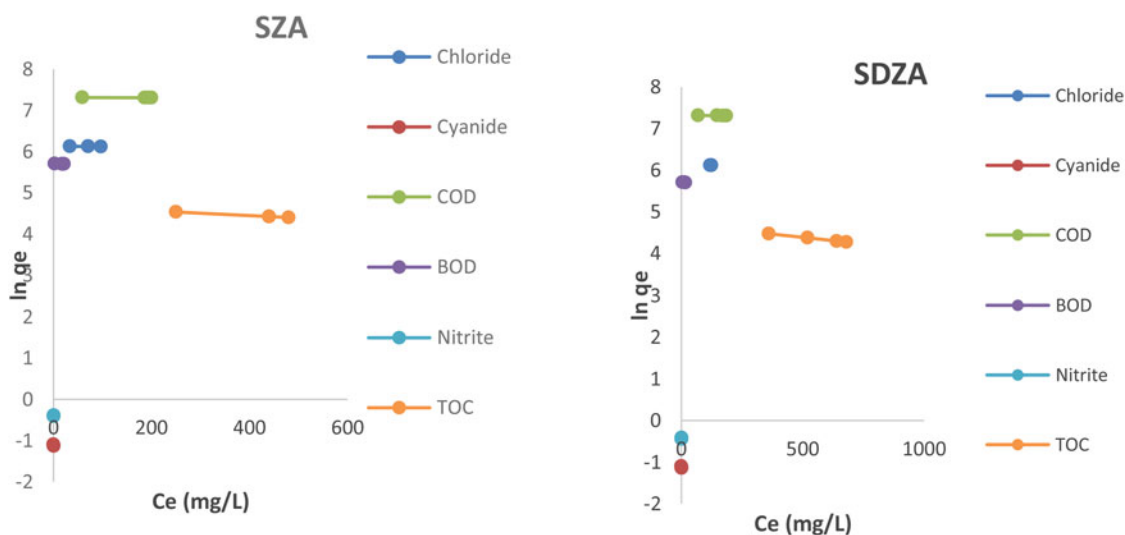


Figure 12. Jovanovic plots of chemical parameters onto SZA and SDZA.

shown in Tables 4 and 5, which suggests that SDZA has higher affinity for removal of the aforementioned chemical parameters. Furthermore, the experimental adsorption capacity ( $q_{e(\text{exp})}$ ) for SZA are 455.1 mg/L, 0.334 mg/L, 1500.7 mg/L, 300.56 mg/L, 0.660 mg/L and 87.5 mg/L for chloride, cyanide, COD, BOD, nitrite and TOC accordingly, while that of SDZA are 459.37 mg/L, 0.335 mg/L, 1501.2 mg/L, 300.68 mg/L, 0.680 mg/L and 93 mg/L for chloride, cyanide, COD, BOD, nitrite and TOC correspondingly as shown in Tables 4 and 5. This suggests that the  $q_m$  for both SZA and SDZA are reasonably in agreement with

$q_{e(\text{exp})}$ . Even though, the  $q_m$  of these pollutants are closer to the ( $q_{e(\text{exp})}$ ) for SZA than SDZA aside from nitrite and TOC as earlier stated, the  $R^2$  values still suggest the best fitting by SDZA indicating the good correlations between the experimental and calculated values. The  $q_m$  values of SZA competing with SDZA might be due to the negligible forces of interaction between adsorbed molecules as assumed by this model (Shahbeig et al., 2013). The disparity in their values is as a result of different concentrations initially present in the solution. The Langmuir adsorption coefficient,  $k_L$ , which is related to energy of sorption, indicated high values

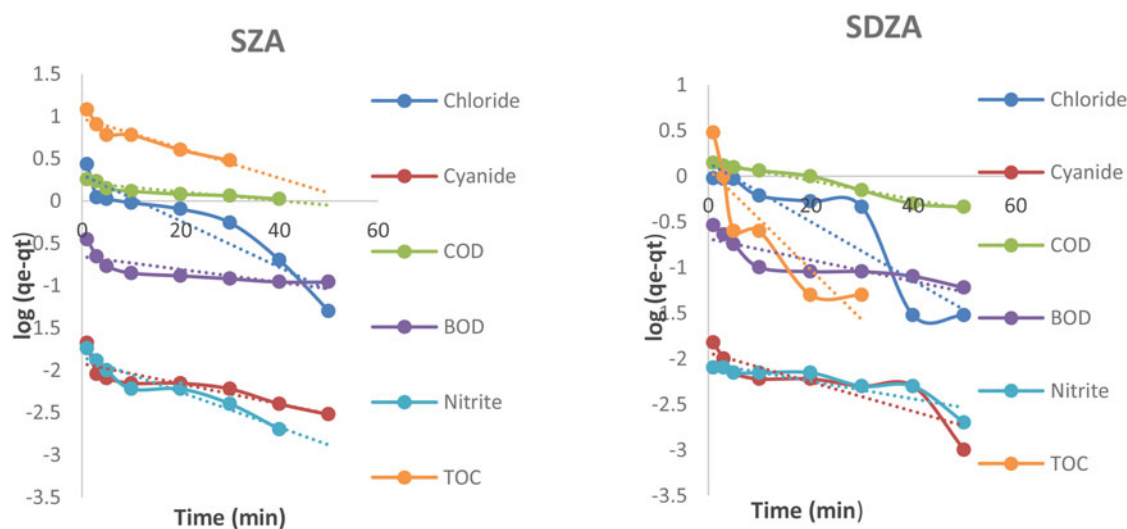


Figure 13. Pseudo-first order kinetics for SZA and SDZA.

Table 4. Isotherms constants for the adsorption of chemical parameters onto SZA.

Adsorption Isotherm	Chloride	Cyanide	COD	BOD	Nitrite	TOC
<b>Langmuir</b>						
$q_{exp}$ (mg/g)	455.1	0.334	1500.7	300.56	0.66	87.5
$q_m$ (mg/g)	454.55	0.32	1428.57	303.03	0.62	59.52
$K_L$ (L/g)	0.611	454.60	2.33	66.00	31.82	0.008
$R$	0.0002	0.000328	0.000014	$0.003 \times 10^{-3}$	0.0022	0.0541
$R^2$	1	0.9999	1	1	1	0.9972
<b>Freudlich</b>						
$1/n$	0.0133	0.0167	0.0038	0.0002	0.0504	0.3137
$K_f$ (L/g)	0.429	0.299	0.503	0.394	0.708	0.439
$R^2$	1	0.9447	0.9904	0.9315	0.9950	0.9883
<b>Harkin-Jura</b>						
$B$	13.333	13.972	50.000	125.00	4.492	2.5
$A$	3,333.33	1.388	$12.5 \times 10^9$	$12.5 \times 10^6$	1.825	5000
$R^2$	1	0.937	0.9902	0.9733	0.9940	0.9741
<b>Jovanovic</b>						
$q_j$ (mg/g)	461.047	0.335	1,504.175	300.666	0.685	107.23
$k_j$	0.0001	0.1523	$3 \times 10^{-5}$	0.0002	0.0744	0.0006
$R^2$	1	1	1	1	1	0.9993

Table 5. Isotherms constants for the adsorption of chemical parameters onto SDZA.

Adsorption Isotherm	Chloride	Cyanide	COD	BOD	Nitrite	TOC
<b>Langmuir</b>						
$q_{exp}$ (mg/g)	459.37	0.335	1501.2	300.68	0.680	93.00
$q_m$ (mg/g)	454.55	0.32	1,428.57	303.03	0.66	72.46
$K_L$ (L/g)	2.44	1,098.06	2.69	110.00	274.50	0.02
$R$	0.00004	0.00014	0.00001	$0.002 \times 10^{-3}$	0.00027	0.00257
$R^2$	1	0.9999	1	1	1	0.9995
<b>Freudlich</b>						
$1/n$	0.0062	0.0109	0.0031	0.0014	0.0170	0.1965
$K_f$ (L/g)	0.427	0.306	0.503	0.394	0.735	0.388
$R^2$	0.9752	0.9499	0.9988	0.9863	0.9897	0.9967
<b>Harkin-Jura</b>						
$B$	50.00	21.265	50.00	142.857	13.401	2.00
$A$	$10^6$	2.158	$12.5 \times 10^7$	$14.286 \times 10^6$	5.747	1000
$R^2$	0.9745	0.9456	0.9987	0.9861	0.9887	0.9933
<b>Jovanovic</b>						
$q_j$ (mg/g)	461.093	0.335	1,504.175	300.786	0.686	109.97
$k_j$	0.0001	0.153	$3 \times 10^{-5}$	0.0002	0.0768	0.0006
$R^2$	1	1	1	1	1	0.9999

for cyanide; 454.60 L/mg and 1098.06 L/mg corresponding to SZA and SDZA, respectively, as observed in the tables. This further confirmed the strong attraction between cyanide and the surfaces of the adsorbents especially the doped zeolite A. From Table 4, the  $k_L$  value of SZA for chloride was 0.611 L/g which is less than 2.44 L/g of SDZA (Table 5). Also, as presented in Table 5, with respect to COD, the  $k_L$  values are 2.69 L/g for SDZA which is higher than 2.33 L/g obtained by SZA (Table 4). According to the tables, BOD exhibited the  $k_L$  value of 110 L/g by SDZA which is greater than 66 L/g by SZA. This observation of SDZA exhibiting the higher energy of sorption in all cases in this study is an indication that a relationship existed between the energy of adsorption  $k_L$  and adsorption capacity  $q_m$ ; Thus, the higher the  $k_L$  for a particular contaminant, the more the strength to bind onto the surface of the adsorbent, subsequently leading to higher removal. An important parameter of the Langmuir isotherm which was expressed as a dimensionless factor  $R$  was also evaluated. The separator factor  $R$  was used in identifying the favorability of the adsorption process, thus, when  $R > 1$  is unfavorable,  $R = 1$  is linear and  $0 < R < 1$  is favorable. From Tables 4 and 5, the values of the separation factor  $R$  are in the range of 0 to  $< 1$ , suggesting that the adsorptions of the contaminants onto the adsorbents are favorable. All the coefficients of regression  $R^2$  ranges from 0.9953 to 1, confirming the monolayer coverage of the contaminants onto the surfaces of the adsorbents as well as their active sites being homogeneously distributed.

The adsorption of the contaminants onto the heterogeneous surfaces of the synthesized adsorbents were also examined using the Freundlich isothermal model and the adsorption parameters are presented in the Tables 4 and 5 for the SZA and SDZA, respectively. The values of  $1/n$  which is related to the intensity of adsorption are in the range of zero to  $< 1$ , suggesting that they have strong surface heterogeneity since their values are close to 0. These values satisfy the condition  $0 > 1/n > 0$ , thus, the closer the value to zero, the stronger the surface heterogeneity (Foo and Hameed, 2010; Margeta et al., 2013). On the other hand,  $k_f$  is related to the adsorption capacity of the adsorbents,

the presented results showed that the sorption capacity of SDZA was greater than SZA for cyanide (0.306 L/g) and nitrite (0.735 L/g) while the two adsorbents have the same affinity towards COD (0.503 L/g) and BOD (0.394 L/g). The adsorption capacity of chloride (0.429 L/g) by SZA was higher than 0.427 L/g by SDZA. The coefficient of regression  $R^2$  of the sorption of chemical parameters from textile effluent onto the adsorbents were in the range of 0.9315–0.9967 except for SZA, which was 1 for chloride. This shows that sorption of chloride for SZA fitted the Freundlich isotherm model correctly; therefore, there was formation of multilayer coverage of chloride on the surfaces of the adsorbents (Margeta et al., 2013). While the  $R^2$  of others suggested that their adsorption mode was not heterogeneous in nature since their  $R^2$  values were less than that of the Langmuir isotherm.

The multilayer adsorption of the pollutants onto heterogeneous pore distributed adsorbents was tested using the Harkins–Jura isotherm. The results are presented in the Tables 4 and 5. According to the tables, equilibrium data for removal of chloride by SZA is well correlated with the Harkins–Jura isotherm as indicated by its good coefficient of regression of 1. However, the low  $R^2$  values of others suggest that the sorption did not follow a multilayer process and the pores of the adsorbents were not heterogeneously distributed.

The homogeneous distribution of the sorbent sites with monolayer coverage and existence of mechanical interaction between the adsorbents-adsorbates were examined using the Jovanovic isotherm model and the Jovanovic constants were evaluated as shown in Tables 4 and 5. With respect to the tables,  $q_j$ , which is associated with the maximum adsorption capacity of SDZA for chloride was 461.093 mg/g which is slightly higher than 461.047 mg/g for SZA. The same capacities were observed by the two adsorbents in the tune of 0.335 mg/g for cyanide, 1504.175 mg/g for COD and 300.786 mg/g for BOD. The disparity in their figures as noticed was due to their initial concentration in the textile effluent. The  $q_j$  for nitrite and TOC for SDZA are 0.686 mg/L and 109.97 mg/L, respectively, which are higher than 0.685 mg/L and 107.23 mg/L for nitrite and TOC, respectively, by SZA. Furthermore, the  $q_j$  for jovanovic isotherm are higher than  $q_m$  for Langmuir isotherm and the



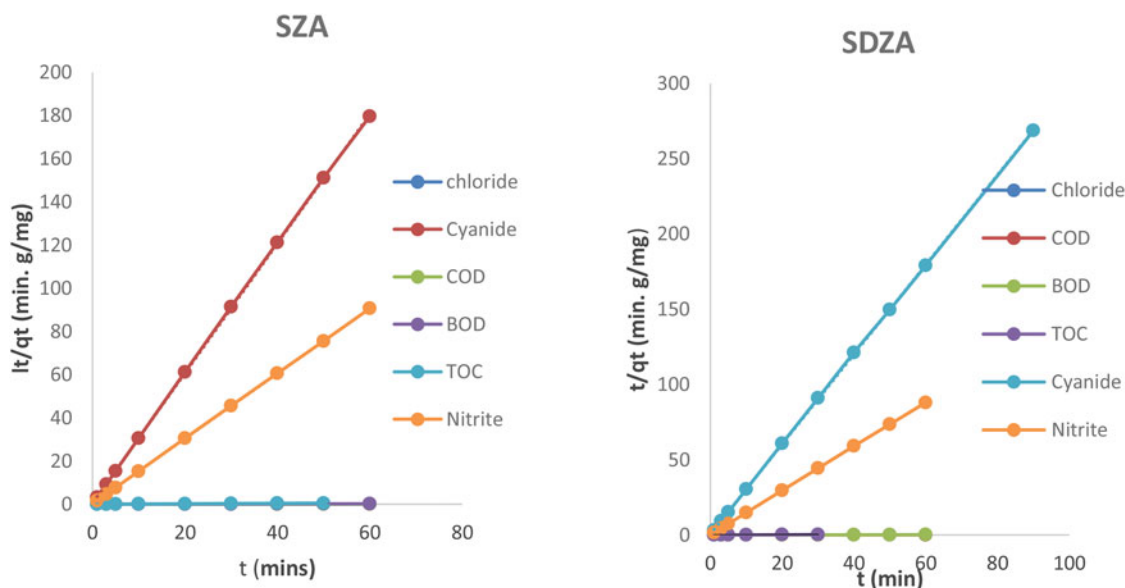


Figure 14. Pseudo-second order kinetics for SZA and SDZA.

$q_j$  for the SDZA are very consistent with the  $q_{e(\text{exp})}$  as presented in the tables. This suggests that the equilibrium data of the chemical parameters by these adsorbents fitted the Jovanovic isotherm best with their  $R^2$  values of 0.999–1. This further confirmed the monolayer coverage of the chemical parameters onto the surfaces of the synthesized adsorbents, though with mechanical interaction existing between them.

In conclusion, the interaction between the synthesized adsorbents and chemical parameters of the textile wastewater according to Tables 4 and 5 in decreasing order of fitness are Jovanovic > Langmuir > Freundlich > Harkins–Jura. The Jovanovic isotherm being the best fit, suggests that the sorption of chemical parameters onto the surface of the described adsorbents followed monolayer coverage with mechanical contacts between them. Furthermore, the SDZA have demonstrated strong interactions compared to the SZA between the contaminants. The strong interaction demonstrated by the doped zeolite might be as a result of the nanoparticles incorporated onto the surface of the SZA for enhancement of its surface area for better adsorption.

### Adsorption kinetics

The mechanism and rate-controlling steps of the chemical parameters onto the zeolites were investigated using the pseudo-first order model, pseudo-

second order model and intraparticle diffusion model (Figures 14 and 15). Their various equations were earlier stated (Equations 12, 13, and 15) and their various results are presented in Table 6.

The pseudo-first order and pseudo-second order models were investigated in this work as shown in the Table 6. According to the table, the pseudo-first order parameters  $q_e$  which is related to the sorption capacity are not in agreement with the experimental values. Also, the coefficients of regression are low ranging from 0.638 to 0.980. On the other hand, the calculated  $q_e$  values of the pseudo-second order model are reasonably in agreement with the experimental values, although, the values of rate constants ( $k_2$ ) are not consistent which may be as a result of its dependency on the initial concentration of the contaminants in solution or due to its identification as a complex function (Markovic et al., 2014). The coefficients of regression ( $R^2$ ) values are 0.996–1 and 1 for SZA and SDZA, respectively, suggesting the fitness to this kinetic order. Therefore, the adsorption of chemical parameters onto the synthesized zeolites may be chemisorption in nature, thus, conformed to the pseudo-second order kinetic model.

Generally, zeolites can take up negatively charged ions, positively charged ions, non-ionic and polar pollutants from wastewater through ion exchange, diffusion processes and adsorption (Srinivasan, 2011). Furthermore, the adsorption of ions on porous adsorbents may involve three

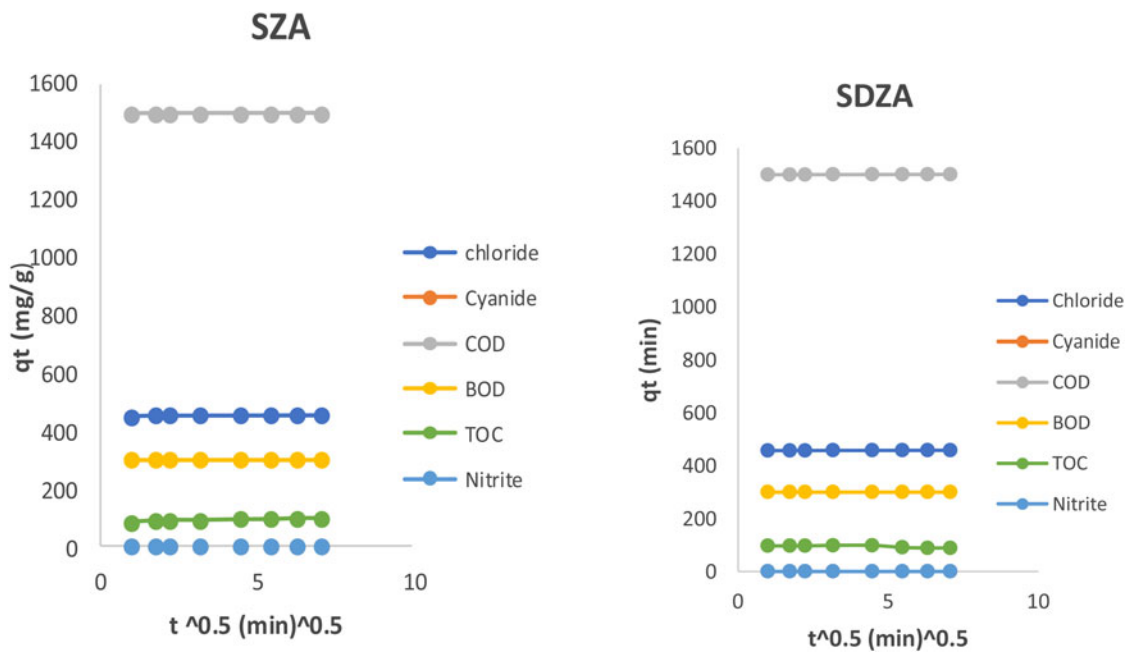


Figure 15. Intraparticle diffusion plots of chemical parameters onto (a) SZA and (b) SDZA.

Table 6. Kinetic constants for the adsorption of chemical parameters onto SZA and SDZA.

Contaminants	Pseudo-first order			Pseudo-second order				
	$k_1$ ( $\text{min}^{-1}$ )	$q_e$ (mg/g)	$R^2$	$k_2$ ( $\text{min}^{-1}$ )	$q_{\text{ecal.}}$ (mg/g)	$q_{\text{eexp}}$ (mg/g)	$r_i$ (mg/g.min)	$R^2$
SZA								
Chloride	0.063	3.257	0.884	0.121	454.55	455.10	$25 \times 10^3$	1
Cyanide	0.027	0.520	0.767	15.686	0.332	0.334	1.739	0.9999
COD	0.012	4.726	0.817	0.490	1,428.57	1500.7	$1000 \times 10^3$	1
BOD	0.018	1.522	0.638	0.545	303.30	300.57	$50 \times 10^3$	1
Nitrite	0.035	0.542	0.915	15.221	0.662	0.660	6.671	1
TOC	0.041	1.029	0.874	0.021	100.00	87.5	212.77	0.9996
SDZA								
Chloride	0.074	6.906	0.843	0.133	500.00	459.37	$33 \times 10^3$	1
Cyanide	0.037	0.517	0.743	13.143	0.335	0.335	1.475	1
COD	0.024	6.321	0.980	0.224	1,492.54	1501.20	$500 \times 10^3$	1
BOD	0.027	1.462	0.786	0.90	333.33	300.68	$100 \times 10^3$	1
Nitrite	0.022	0.487	0.786	17.110	0.681	0.680	7.935	1
TOC	0.127	12.771	0.781	0.150	105.26	93.00	$1.67 \times 10^3$	1

steps; diffusion of the ions to the adsorbent surface, diffusion of ions into the pores of the adsorbents and adsorption of the ions on the internal surface of adsorbents (Al-Anber, 2011).

Thus, for the adsorption of BOD, COD, and TOC, their ions from the wastewater adhere to the adsorbents surface and ion-exchange mechanism occurred while the adsorption mechanism of Cl, CN,  $\text{NO}_2$  are through diffusion of their ions into the pores of the developed adsorbents, followed by their adsorption in the internal surfaces. This might be due to the sizes of these pollutants (cyanide= 0.177 nm, nitrite= 0.155 nm and chloride= 0.184 nm) which are smaller than the pore diameters of the developed adsorbents (SZA

= 3.328 nm and SDZA= 5.90 nm), thereby, making their entrapment possible in their pores. This mechanism was also explained by the conformity to pseudo-second order kinetics and intraparticle diffusion model studied.

The intraparticle diffusion model developed by Morris and Weber was used to investigate if the adsorption of chemical parameters is controlled by intraparticle diffusion. This model can only be understood with the help of mathematical graphs, as such the plots of  $q_t$  against  $t^{0.5}$  are shown in Figures 15(a) and 15(b), respectively, for SZA and SDZA.

Figures 15(a) and 15(b) show a straight line graph suggesting that the adsorption of chemical

parameters onto synthesized adsorbents involved intraparticle diffusion of the micropore type. Though, intraparticle diffusion was not the sole rate-limiting step as the graph did not pass through the origin (Yakout and Elsherif, 2010). Besides, deviation from the origin also signifies some degree of boundary layer which implied that other kinetic models were associated with control of the sorption.

The intraparticle parameters were evaluated from the slopes and intercepts of the plots and results are presented in the Table 7.

From Table 7, the intraparticle coefficient  $C$ , is related to sorption capacity and their values correlated well with the experimental values. The results also show that the maximum sorption capacity was achieved by SDZA. The reason is the same as stated earlier.

### Thermodynamics of adsorption

The thermodynamic parameters such as Gibb's free energy,  $\Delta G^\circ$ , the enthalpy  $\Delta H^\circ$  and the

entropy  $\Delta S^\circ$  were also evaluated as they represent the vital index for the practical applications of a process. The parameters were determined from the Equations (18) and (19) and the  $K$  was obtained from Equation 20 (Liu, 2009; Bankole et al., 2017)

$$K = C_{ads} / C_e \quad (20)$$

$K$  is the equilibrium constant;  $C_{ads}$  and  $C_e$  are the equilibrium concentrations of the chemical parameters (mg/L) in solution and on the adsorbents, respectively. The plots of  $\ln K$  vs.  $1/T$  are shown in the Figures 16 and 17.

$\Delta H^\circ$  and  $\Delta S^\circ$  were evaluated from the slopes and intercepts of the plots as presented in the Table 8.

It can be deduced from Table 8 that the sorption of chemical parameters onto the surfaces of the synthesized adsorbents involved endothermic reactions as indicated by the positive values of  $\Delta H^\circ$ . This further confirmed the result of the adsorption isotherm and kinetic studies which both suggested monolayer coverage and chemisorption process. Endothermic reactions have been identified to associate with monolayer coverage (Grassi et al., 2012) and increase in the adsorption capacity of the chemical parameters with increase in temperature observed in the course of studying the effect of temperature on their adsorption capacities further support these results. Also, the positive values of  $\Delta S^\circ$  for the removal of chemical parameters from the textile wastewater are indications that the degree of disorder increased at the solid-solution interface (Piccin et al., 2011) in the course of the

Table 7. Intraparticle diffusion model.

Contaminants	$K_m$ (mg/g.min <sup>0.5</sup> )	$C$ (mg/g)	$R^2$
SZA			
Chloride	0.3114	452.96	0.7339
Cyanide	0.0019	0.3182	0.6143
COD	0.1235	1498.90	0.8935
BOD	0.0355	300.26	0.8228
Nitrite	0.0026	0.6447	0.8993
TOC	1.7313	81.813	0.9173
SDZA			
Chloride	0.1628	458.10	0.9314
Cyanide	0.0016	0.3218	0.7646
COD	0.1629	1499.80	0.9721
BOD	0.0174	300.51	0.7593
Nitrite	0.0008	0.6727	0.8105
TOC	1.534	98.52	0.5639

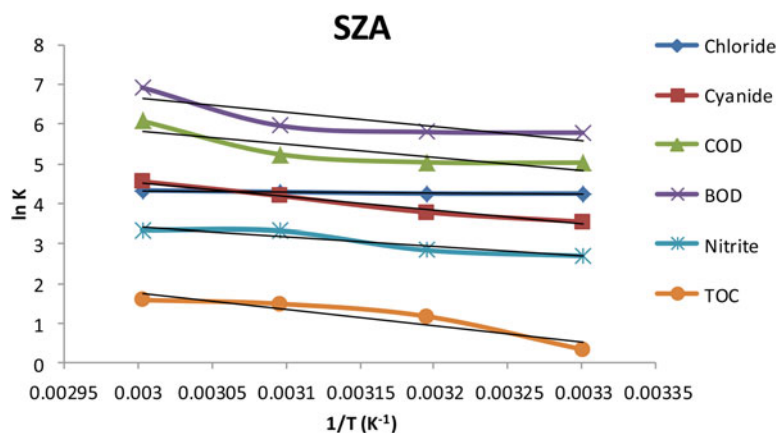


Figure 16. Plot of  $\ln K$  vs.  $1/T$  for SZA.

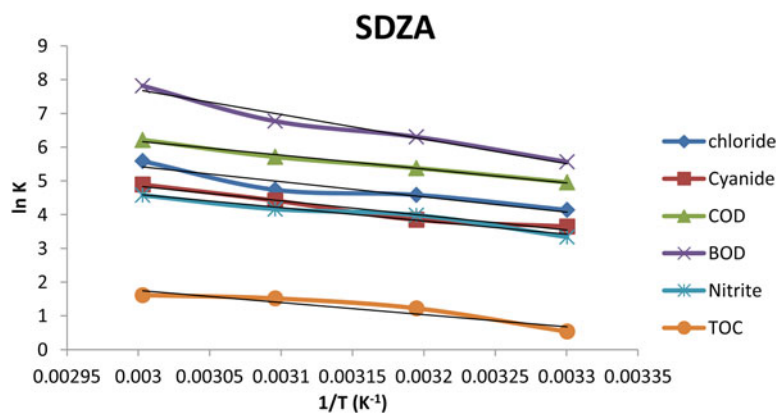


Figure 17. Plot of  $\ln K$  vs.  $1/T$  for SDZA.

Table 8. Thermodynamic parameters of adsorption of chemical parameters onto SZA and SDZA.

Contaminants	SZA		SDZA	
	$\Delta H^\circ$ (kJ/mol)	$\Delta S^\circ$ (J/mol)	$\Delta H^\circ$ (kJ/mol)	$\Delta S^\circ$ (J/mol)
Chloride	2.352	42.971	37.477	157.575
Cyanide	28.972	124.595	35.857	147.823
COD	27.608	131.345	34.389	154.541
BOD	29.440	143.525	60.477	245.396
Nitrite	20.351	89.392	32.696	136.325
TOC	34.377	117.735	29.970	104.524

Table 9.  $\Delta G^\circ$  values of sorption chemical parameters onto SZA and SDZA at different temperatures.

Contaminants	30 °C	40 °C	50 °C	60 °C
	$\Delta G^\circ$ (kJ/mol)	$\Delta G^\circ$ (kJ/mol)	$\Delta G^\circ$ (kJ/mol)	$\Delta G^\circ$ (kJ/mol)
SZA				
Chloride	-10.668	-11.098	-11.527	-11.957
Cyanide	-8.777	-10.023	-11.268	-12.514
COD	-12.189	-13.503	-14.816	-16.129
BOD	-14.048	-15.483	-16.919	-18.354
Nitrite	-6.734	-7.628	-8.522	-9.416
TOC	-1.297	-2.474	-3.651	-4.828
SDZA				
Chloride	-10.267	-11.843	-13.419	-14.995
Cyanide	-8.933	-10.411	-11.889	-13.368
COD	-12.436	-13.982	-15.527	-17.073
BOD	-13.878	-16.332	-18.786	-21.240
Nitrite	-8.611	-9.974	-11.337	-12.701
TOC	-1.700	-2.746	-3.791	-4.836

adsorption process.  $\Delta G^\circ$  at different temperatures were also calculated from the Equation (16) and the results are presented in Table 9.

The negative values of  $\Delta G^\circ$  as shown in Table 9 indicated that the adsorptions of chemical parameters onto synthesized adsorbents were spontaneous and the spontaneity increased with temperature. Thus, at higher temperature, the adsorption of chemical parameters increased. In addition, the increase in the values of  $K_c$  with temperature as observed in Table 10 for both adsorbents suggest that the force of attraction between the adsorption sites of the adsorbents

Table 10.  $K$  values of sorption of chemical parameters onto SZA and SDZA at different temperatures.

Contaminants	30 °C	40 °C	50 °C	60 °C
	K	K	K	K
SZA				
Chloride	69.930	69.930	72.768	75.841
Cyanide	34.263	43.667	66.000	94.714
COD	152.235	153.814	187.893	434.275
BOD	324.189	329.549	387.129	1010.092
Nitrite	14.747	17.026	27.542	28.149
TOC	1.398	3.220	4.410	4.861
SDZA				
Chloride	62.593	97.832	113.832	266.275
Cyanide	38.412	46.857	82.750	133.000
COD	142.019	216.638	302.373	499.567
BOD	260.565	545.909	870.884	2484.950
Nitrite	28.149	53.800	64.238	96.857
TOC	1.705	3.396	4.553	5.026

and the contaminants as well as the adjacent molecules of the adsorbed phases increased with temperature (Bankole et al., 2017). Furthermore, the high value of  $K_c$  is an indication of spontaneous reactions between the adsorbents and the pollutants except for TOC which suggest otherwise. According to the website of City Collegiate, the occurrence of its reactions may be in both forward and backward direction resulting to moderate values of  $K_c$  ([http://www.citycollegiate.com/chemical\\_equilibrium3.htm](http://www.citycollegiate.com/chemical_equilibrium3.htm)). The values of  $K_c$  of SDZA higher than SZA show that the doped adsorbent is stronger in removal of these pollutants than the undoped adsorbent.

## Conclusions

In this study, zeolite A was produced from kaolin while green synthesis of silver nanoparticles was carried out with mango leaf extract as a reducing agent. The silver nanoparticle was doped onto the surface of zeolite A to produce a Nano

adsorbent for local textile wastewater treatment. The synthesized adsorbents were characterized using XRD, XRF, SEM, TEM, FT-IR, and BET surface analyzer. The XRD results revealed well crystalline adsorbents and the surface area of the SZA and SDZA were  $119.98 \text{ m}^2/\text{g}$  and  $436.44 \text{ m}^2/\text{g}$ , respectively. The adsorption of chemical parameters from textile wastewater onto SZA and SDZA were rapid removing 82.94–99.81% and 92.42–99.90%, respectively, within the first minute. It also showed that the adsorption increased with contact time, adsorbent dosage and temperatures by both SZA and SDZA. Isothermal models indicated the suitability of the Jovanovic model in describing the adsorption process and it conforms to pseudo-second order kinetics. In addition, the adsorption of chemical parameters onto the surfaces of the synthesized adsorbents involved intraparticle diffusion of micropore type. The thermodynamic studies showed spontaneous reactions which were endothermic in nature. It can be informed from various analysis conducted that the developed adsorbents are suitable for textile wastewater treatments with SDZA performing better than SZA.

### Disclosure statement

No potential conflict of interest was reported by the authors.

### References

- Acemioglu, B. (2010). Adsorption of Congo red from aqueous solution onto calcium-rich ash, *J. Coll. Interface Sci.*, **2010**, 273–371.
- Al-Anber, M. A. (2011). Thermodynamics approach in the adsorption of heavy metals. In *Thermodynamics - Interaction Studies - Solids, Liquids and Gases*, ed Dr. Juan Carlos Moreno Piraján, 736–761, InTech. ISBN: 978-953-307-563-1.
- Al-Asheh, S., Banat, F., and Abu-Aitah, L. (2003). Adsorption of phenol using different types of activated bentonites, *Sep. Purif. Technol.*, **33**, 1–10.
- Allafchian, A. R., Mirahmadi-Zare, S. Z., Jalali, S. A. H., Hashemi, S. S., and Vahabi, M. R. (2016). Green synthesis of silver nanoparticles using *phlomis* leaf extract and investigation of their antibacterial activity, *J. Nanostruct. Chem.*, **6**, 129–135.
- Ayawei, N., Ebelegi, A. N., and Wankasi, D. (2017). Modelling and interpretation of adsorption isotherms, *J. Chem.*, **2017**, 1–11.
- Bankole, M. T., Abdulkareem, A. S., Tijani, J. O., Ochigbo, S. S., Afolabi, A. S., and Roos, W. D. (2017). Chemical oxygen demand removal from electroplating wastewater by purified and polymer functionalized carbon nanotubes adsorbents, *Water Resour. Ind.*, **18**, 33–50.
- Bertolini, T. C. R., Izidoro, J. C., Magdalena, C. P., and Fungaro, D. A. (2013). Adsorption of crystal violet dye from aqueous solution onto zeolites from coal fly and bottom ashes, *Orbital- Electr. J. Chem.*, **5**, 179–191.
- Byrappa, K., and Suresh Kumar, B. V. (2007). Characterization of zeolites by infrared spectroscopy, *Asian J. Chem.*, **19**, 4933–4935.
- Cejka, J., Bekkum, H. V., Corma, A., and Scuth, F. (2007). *Introduction to Zeolite Science and Practice, Study of Surface Science Catalysis*, 3rd revised ed., Elsevier, Amsterdam.
- Chouhan, N., Sharma, A., Kumar, A., and Ameta, R. (2013). Chapter 3 “Eco-friends products.” In *Green Chemistry: Fundamentals and Applications*, 1st ed., ed. Taylor and Francis, 43–86, Apple Academia Press CRC.
- Dada, A. O., Olalekan, A. P., Olatunya, A. M., and Dada, O. (2012). Langmuir, Freundlich, Temkin, and Dubinin-Radushkevich isotherms studies of equilibrium sorption of  $\text{Zn}^{2+}$  onto phosphoric acid modified rice husk, *J. Appl. Chem.*, **3**, 38–45.
- Deepak, V., Kalishwaralal, K., Pandian, S. R. K., and Gurunnalhen, A. (2011). An insight into bacterial biogenesis of silver nanoparticles, industrial production and scale-up. In *Metal Nanoparticles in Microbiology*, eds Rai M. and Duren N., 17–35, Springer-Verlag, Berlin Heidelberg.
- Destá, M. B. (2013). Batch adsorption experiments: Langmuir and Freundlich isotherm studies for the adsorption of textile metal ions onto Teff straw (*Eragrostis tef*) agricultural waste, *J. Therm.*, **2013**, 1–6.
- Dey, S., and Islam, A. (2015). A review on textile wastewater characterization in Bangladesh, *Res. Environ.*, **5**, 15–44.
- Diaz-Nava, C., Olgium, M. T., and Solaclu-Rois, M. (2002). Water defluoridation by Mexican Heulandite-Clipnotilolite, *Sep. Sci. Tech.*, **37**, 3109–3128.
- Elango, G., Rathika, G., and Elango, S. (2017). Physicochemical parameters of textile dyeing effluent and its impact with case study, *Int. J. Res. Chem. Environ.*, **7**, 17–24.
- Fierro, V., Torné-Fernández, V., Montané, D., and Celzard, A. (2008). Adsorption of phenol onto activated carbons having different textural and surface properties, *Micropor. Mesopor. Mater.*, **111**, 276–288.
- Fondriest Environmental Inc. (2013). Dissolved oxygen. In *Fundamentals of Environmental Measurements*. <http://www.fondriest.com/environmentalmeasurements/parameters/water-> >.



- Foo, K. Y., and Hameed, B. H. (2010). Insight of the modeling of adsorption isotherm systems, *Chem. Eng. J.*, **156**, 2–10.
- Freundlich, H. M. F. (1906). Over the adsorption in solution, *J. Phys. Chem.*, **57**, 385–470.
- Gougazeh, M., and Buhl, J. C. (2014). Synthesised and characterization of zeolite a by hydrothermal transformation of natural Jordanian kaolin, *J. Assoc. Arab Univ. Basic Appl. Sci.*, **15**, 35–42.
- Gougazeh, M., and Buhl, J. C. (2010). Geochemical and mineralogical characterization of the Jabal Al-Harad kaolin deposit, Southern Jordan for its possible utilization, *Clay Miner. Miner.*, **45**, 301–314.
- Grassi, M., Kaykioglu, G., Belgioino, V., and Lofrano, G. (2012). Removal of emerging contaminants from water and wastewater by adsorption process. In *Emerging Compounds Removal from Wastewater, Chapter 2.*, ed. G. Lofrano, 15–37, Springer Briefs in Green Chemistry for Sustainability.
- Guidelines for Drinking Water Quality, World Health Organization (WHO) (2011), 4th ed., 120–350, WHO Press, Geneva, Switzerland. ISBN 978-92-4-15481.5, NLM Classification: WA 675.
- Hall, K. R., Eagleton, L. C., Acrivers, A., and Vermenlem, T. (1966). Industrial engineering, *Chem. Res.*, **5**, 212.
- Johnson, E. B. G., Arshad, S. E., and Asik, J. (2014). Hydrothermal synthesis of zeolite a using natural kaolin from KG grading Bongawon Sabeh, *J. Appl. Sci.*, **14**, 3282–3328.
- Juliano, C., and Magrini, G. A. (2017). Cosmetics ingredients as emerging pollutants of environmental and health concern. A mini review, *Cosmetics*, **4**, 11–18.
- Kamyar, S., Mansor, A., Mohsen, Z., Wan Md Zin, W. Y., and Nor, A. J. (2011). Fabrication of silver nanoparticles doped in the zeolite framework and antibacterial activity, *Int. J. Nanomed.*, **6**, 331–341.
- Kant, R. (2011). Textile dyeing industry and environmental hazard, *Nat. Sci.*, **4**, 22–26.
- Kovo, A. S. (2012). Effects of temperature on the synthesis of zeolite X from Ahoko Nigerian kaolin using novel metakaolinization technique, *Chem. Eng. Comm.*, **199**, 786–787.
- Kovo, A. S. (2011). Development of zeolites and zeolites membranes from Ahoko Nigerian Kaolin (Ph.D. thesis, University of Manchester, UK).
- Langmuir, I. (1918). The adsorption of gases on plane surface of glass, mica and platinum, *J. Am. Chem. Soc.*, **40**, 1361–1368.
- Liu, Y. (2009). Is the free energy change of adsorption correctly calculated, *J. Chem. Eng. Data*, **54**, 1981–1985.
- Mabape, K. I. S. (2017). Assessment of the potentials of selected adsorbents for use in small scale system for the removal of Uranium from mine-impacted water (A master's thesis submitted to the faculty of science, University of Witwatersrand, Johannesburg).
- Margeta, K., Logar, N. Z., Siljeg, M., and Farkes, A. (2013). A natural zeolite in water treatment- How effective is their use, *INTECH.*, **5**, 81–111.
- Markovic, D. D., Lekic, B. M., Rajakovic-Ognjanovic, V. N., Onijia, A. E., and Rajakovic, L. V. (2014). A new approach in regression analysis for modelling adsorption isotherm, Hindawi publishing corporation, *Sci. World J.*, **2014**, 1–17.
- Mates, A., Kovacevic, D., Vujevic, D., and Papie, S. (2004). The role of zeolites in wastewater treatment of printing inks, *Water Res.*, **28**, 3373–3381.
- Mirfendereski, M., and Mohammed, T. (2016). Effects of synthesis parameters on the characterization of Naa Type zeolite. Paper presented at the World Congress on Recent Advances in Nanotechnology.
- Mittal, A. K., Chisti, Y., and Banerjee, U. C. (2013). Synthesis of metallic nanoparticles using plant extracts, *Biotechnol. Adv.*, **31**, 346–356.
- Muthoosany, K., Bai, R. G., Abubakar, I. B., Sudheer, S. M., Lim, H. N., Loh, H. S., Huang, N. M., Chia, C. H., and Manickam, S. (2015). Exceedingly biocompatible & thin-layered reduced graphene oxide nanosheets using eco-friendly mushrooms extract strategy, *Int. J. Nanomed.*, **10**, 1505–1519.
- Nigerian Standard for Drinking Water Quality.* (2007). Standard Organization of Nigeria (SON), Nigerian Industrial Standard; NIS SS4, ICS 13.060-20, 1–29.
- Parameters of water quality; Interpretation and Standards.* (2001). Environmental Protection Agency, Johnstown Castle, Co. Wexford, Ireland, ISBN 1- 84096-015-3, 27–116.
- Odutayo, F. O. I., Oyetade, O. B., and Adaramola, F. B. (2016). Effects of industrial effluents on the environment using *Allium cepa* and *Zea mays* as bioindicators, *Int. J. Environ. Pollut. Res.*, **4**, 1–12.
- Patel, R., Tajddin, K., Patel, A., and Patel, B. (2015). Physico-chemical analysis of textile effluent, *Int. J. Res. Sci. Innov.*, **2**, 33–37.
- Piccin, J. S., Dotto, G. L., Vierra, M. L. G., and Pinto, L. A. A. (2011). Kinetic and mechanism of the dye FD & C red 40 binding onto chitosan, *Brazilian J. Chem. Eng.*, **28**, 295–304.
- Radnia, H., Ghoreyshi, A., A., and Younesi, H. (2011). Isotherm and kinetics of Fe (II) adsorption onto chitosan in a batch process, *Iranian J. Energ. Environ.*, **2**, 250–257.
- Said- Mansour, M., Kadri, E., Kenai, S., Ghrici, M., and Bennaceur, R. (2011). Influence of calcined kaolin on mortar properties, *Const. Building Mater.*, **25**, 2275–2282.
- Salah El-Din, T. A., Elzatahry, A. A., Aldhayen, D. M., Al-Enizi, A. M., and Al-Deyab, S. S. (2011). Synthesis and characterization of magnetic zeolite nanocomposite, *Int. J. Electrochem. Sci.*, **6**, 6177–6183.
- Sarsar, V., Selwal, K. K., and Selmal, M. K. (2013). Green synthesis of silver nanoparticles using leaf extract of *Mangifera indica* and evaluation of their antimicrobial activity, *J. Microbiol. Biotechnol. Res.*, **3**, 27–32.

- Sekhar, E. C., Krishna Rao, K. S. V., Rao, K. M., and Pradeep, K. S. (2016). A green approach to synthesize controllable silver nanostructures from *Linonia accidis-sima* for inactivation of pathogen bacteria, *Cogent Chem.*, **2**, 1–14.
- Shah, S., Daggupta, S., Chakraborty, M., Vadakkekara, R., and Hajoori, M. (2014). Green synthesis of iron nanoparticles using plant extracts, *Int. J. Biol. Pharm. Res.*, **5**, 549–552.
- Shahbeig, H., Baghen, N., Ghorbanion, S. A., Hallajisani, A., and Poorkarimi, S. (2013). A new adsorption isotherm model of aqueous solutions on granulated activated carbon, *World J. Model. Simul.*, **9**, 243–254.
- Shakeel Ahmed, S., Ahmed, M., Swami, B. L., and Ikram, S. (2016). Green synthesis of silver nanoparticles using *Azadiracta indica* aqueous leaf extract, *J. Radiat. Res. Appl. Sci.*, **9**, 1–7.
- Sherrard, J. H., Moore, D. R., and Dillaha, T. A. (1987). Total dissolved solids; Determination, source, effects and removal, *J. Environ. Ed. Res.*, **18**, 19–24.
- Sithra, R., and Sivashanmugam, P. (2017). Economical synthesis of silver nanoparticles using leaf extract of *Acalypha hispida* and its application in the detection of Mn(II) ions, *J. Adv. Res.*, **8**, 561–568.
- Song, J. Y., and Kim, B. S. (2009). Rapid biological synthesis of silver nanoparticles using plant extracts, *Bioprocess Biosyst. Eng. Eng.*, **32**, 79–84.
- Sivakumar, K. K., Balamurugan, C., Ramakrishna, D., and Bhai, L. H. (2011). Assessment studies on wastewater pollution by textile dyeing and bleaching industries at Karur, Tamil Nadu, *Rasayan. J. Chem.*, **4**, 264–269.
- Srinivasan, R. (2011). Advances in application of natural clay and its composites in removal of biological, organic and inorganic contaminants from drinking water, *Adv. Mater. Sci. Eng.*, **2011**, 1–7.
- Tafesse, T. B., Yetemegne, A. K., and Kumar, S. (2015). The physico-chemical studies of water in Hawassa textile industry, *Environ. Anal. Chem.*, **2**, 1–6.
- Thiruvengkatachari, R., Vigneswaran, S., and Naidu, R. (2008). Permeable reactive barrier for groundwater remediation, *J. Ind. Eng. Chem.*, **14**, 145–156.
- Turabik, M. (2008). Adsorption of basic dyes from single and binary component systems onto bentonite; simultaneous analysis of basic red 46 & basic yellow 28 by first order derivative spectrophotometric analysis method, *J. Hazard. Mater.*, **158**, 52–64.
- Varma, L., and Sharma, J. (2011). Analysis of physical and chemical parameters of textile wastewater, *J. Int. Phys. Sci.*, **15**, 269–279.
- Varsha, G., and Singh Seema, J. Physico-chemical analysis of textile effluents of dye and printing clusters of Bagne region, Jaipur, India, *J. Environ. Res. Dev.*, **8**, 11–15.
- Wang, T., Lin, J., Chen, Z., Megharaj, M., and Naidu, R. (2014). Green synthesized iron nanoparticles by green tea and eucalyptus leaves extracts used for removal of nitrate in aqueous solution, *J. Cleaner Prod.*, **83**, 413–419.
- Weber-Scannell, P. K., and Duffy, L. (2007). Effects of total dissolved solids on aquatic organism: A review of literature and recommendations for Salmond species, *Am. J. Environ. Sci.*, **3**, 1–6.
- Yakout, S. M., and Elsherif, E. (2010). Batch kinetic, isotherm and thermodynamic studies of adsorption of strontium from aqueous solutions onto low cost rice straw based carbons, *Carbon Sci. Tech.*, **1**, 144–153.
- Yusuf-Alaya, S. (2014). Synthesis, intercalation and characterization of zeolite A for adsorption studies of methylene blue, 22–45. (Master's thesis, Federal University of Technology, Minna, Niger state, Nigeria).
- Zainal Abidin, A., Abu Bakar, N. H. H., Ng, E. P., and Tan, W. L. (2017). Rapid degradation of methy orange by Ag doped zeolite X in the presence of borohydride, *J. Taibah Univ. Sci.*, **11**, 1070–1079.
- Zavareh, S., Farrokhzad, Z., and Darvish, F. (2018). Modification of zeolite 4A for use as an adsorbent for glyphosate and as antibacterial agent for water, *Ecotoxicol Environ. Saf.*, **155**, 1–8.
- Zhao, H., Deng, Y., Harsh, J. B., Flury, M., and Boyle, J. S. (2004). Alteration of kaolinite to cancrinite and sodalite by simulated Hanford tank waste and its impact on cesium retention, *Clays Clay Miner.*, **52**, 1–13.